



HAL
open science

Unveiling *Crocospaera* responses to phosphorus depletion: insights from genome analysis and functional characterization

Chloé Caille, Sophie Rabouille, Eva Ortega-Retuerta, Yann Denis, Olivier Crispi, Barbara Marie, Mireille Pujon-Pay, Vladimir Daric, Emmanuel Talla, Amel Latifi

► **To cite this version:**

Chloé Caille, Sophie Rabouille, Eva Ortega-Retuerta, Yann Denis, Olivier Crispi, et al.. Unveiling *Crocospaera* responses to phosphorus depletion: insights from genome analysis and functional characterization. 2024. hal-04786428

HAL Id: hal-04786428

<https://hal.science/hal-04786428v1>

Preprint submitted on 15 Nov 2024

HAL is a multi-disciplinary open access archive for the deposit and dissemination of scientific research documents, whether they are published or not. The documents may come from teaching and research institutions in France or abroad, or from public or private research centers.

L'archive ouverte pluridisciplinaire **HAL**, est destinée au dépôt et à la diffusion de documents scientifiques de niveau recherche, publiés ou non, émanant des établissements d'enseignement et de recherche français ou étrangers, des laboratoires publics ou privés.

Unveiling *Crocospaera* responses to phosphorus depletion: insights from genome analysis and functional characterization

Chloé Caille^{1,2}, Sophie Rabouille^{1*}, Eva Ortega-Retuerta¹, Yann Denis³, Olivier Crispi¹, Barbara Marie¹, Mireille Pujol-Pay¹, Vladimir Daric⁴, Emmanuel Talla², and Amel Latifi^{2*}

¹ Sorbonne Université, CNRS, Laboratoire d'Océanographie Microbienne, LOMIC, F-66650 Banyuls-sur-Mer, France.

² Aix Marseille Univ, CNRS, laboratoire de Chimie Bactérienne LCB, IMM, Marseille, France

³ Plateforme transcriptomique, Aix-Marseille Univ., CNRS, IMM, Marseille, France

⁴ Sorbonne Université, CNRS, Biologie Intégrative des Organismes Marins (BIOM), F-66650 Banyuls/Mer, France

* Corresponding authors:

latifi@imm.cnrs.fr; Tel. +33 (0)491 164 298

sophie.rabouille@obs-banyuls.fr; Tel. +33 (0)430 192 444

Running title: *Crocospaera's* responses to phosphate depletion

Keywords: cyanobacteria, *Crocospaera*, diel cycle, gene expression, genomics, phosphorus depletion.

Data available within the article or its supplementary materials

Contributions

Conceptualization: SR, AL. Investigation: ET, CC, SR, AL, OC, BM, EOR, YD, MPP. Formal analysis: ET, AL, SR, CC, VD, YD. Validation: AL, ET, SR, YD. Visualization: CC, ET, AL, SR. Supervision: SR, AL, EOR. Paper writing: AL, SR. Funding acquisition: SR.

Acknowledgments

This study was supported by the LEFE-CYBER (CNRS) program. Work in AL lab was funded by Agence Nationale pour la Recherche Scientifique” (ANR-21-CE20-0025-01). Chloé Caille was funded by a doctoral fellowship from ED129 at Sorbonne University. Flow cytometry analyses were conducted at the SU/CNRS BioPIC Imaging and Cytometry platform of Banyuls Oceanologic Observatory under the technical support of EMBRC-France. We are grateful to the Bio2Mar platform (<http://bio2mar.obs-banyuls.fr>) for providing access to the Victor 3 plate reader. The authors thank Stéphanie Champ for assistance with the RNA extraction procedure. Part of the bioinformatics analyses were performed on the Core Cluster of the Institut Français de Bioinformatique (IFB) (ANR-11-INBS-0013).

40
41
42
43
44
45
46
47
48
49
50
51
52
53
54
55
56
57

58
59
60
61
62
63
64

Abstract

Unicellular, nitrogen-fixing cyanobacteria (UCYN) thrive and support primary production in oligotrophic oceans, playing a significant role in the marine nitrogen cycle. *Crocospaera* sp, a model for studying marine nitrogen fixation, is adapted to low phosphate (P_i) conditions. Yet, how *Crocospaera* copes with P_i depletion is rather poorly understood. We present genomics analysis of P_i stress-responsive genes in this genus, encompassing six *C. watsonii* genomes and two strains isolated in coastal environments, *C. subtropica* and *C. chwakensis*. We identified genes involved in P_i signaling, uptake, and dissolved organic phosphorus (DOP) hydrolysis. Results showed different genetic potentials to cope with P_i scarcity between the *Crocospaera* strains. Physiological monitoring of cultures of *C. watsonii* WH8501 exposed to P_i depletion highlighted a capacity to divide several times and survive for a few more days, albeit with a skewed C:N:P stoichiometry. Upon addition of DOP, cultures efficiently recovered to a growth rate and cell composition equivalent to those observed under favorable conditions. The concomitant transcription analysis revealed diel expression patterns of P_i-related genes and endogenous clock genes, suggesting a possible circadian regulation. Our data deepen our understanding of the growth strategies *Crocospaera* employs in P_i-limited environments, offering broader insights into microbial resilience in marine ecosystems.

65

66 **Introduction**

67

68 Unicellular, nitrogen-fixing cyanobacteria (UCYN) are prevalent in the tropics and subtropics
69 areas of the open ocean, playing a significant role in the marine nitrogen cycle (1). Nitrogen
70 (N) fixation is the primary mechanism introducing new N into the open ocean, supporting up
71 to half of the new primary production (2) (3). This underscores the critical importance of
72 diazotrophic cyanobacteria in these oligotrophic regions. The genus *Crocospaera* is a
73 cultivated representative of open-ocean, photo-autotrophic UCYNs. It is a key model organism
74 for studying N fixation and how this process varies with environmental factors. Based on the
75 phylogenetic distribution of the *nifH* gene, the *Crocospaera* genus has been divided into two
76 clades: the UCYN-B clade, which includes the species *C. watsonii* (4) (5), further subdivided
77 into small and large strains (6). The UCYN-C clade includes *C. subtropica* and *C. chwakensis*,
78 two strains isolated in coastal environments and formerly classified under *Cyanothece* (7). The
79 growth of diazotrophic cyanobacteria can be limited by the availability of nutrients, primarily
80 iron and phosphorus. Nevertheless, *Crocospaera* strains are widely distributed in oligotrophic
81 regions with low phosphorus (P) levels (1). For instance, *in situ* observations indicated that
82 diazotrophic cyanobacteria are present the Southwest Pacific (8) and the Northern tropical
83 Atlantic Oceans (9). Their ecological distribution suggests that *Crocospaera* strains have
84 developed adaptive mechanisms to cope with P_i depletion.

85 Bacterial strategies to adapt to phosphate (P_i) limitation are diverse, including the replacement
86 of phospholipids with sulfolipids, the use of high-affinity P_i transporters (10), and the
87 scavenging of dissolved organic phosphorus (DOP) sources through hydrolytic enzymes (4)
88 (11) (12). Most of these mechanisms are induced in response to P_i depletion, as perceived by
89 the two-component regulatory system of the PhoB-PhoR family (13). Current knowledge on

90 how *Crocospaera* copes with P_i depletion is primarily derived from studies on *C. watsonii*.
91 For example, alkaline phosphatase activity was measured in *C. watsonii* P_i -depleted cultures
92 and this strain can use dissolved organic phosphorus (DOP) as its sole phosphorus source,
93 including phosphomonoesters and phosphodiester (14). However, the transcription of none of
94 the three genes annotated as potentially encoding alkaline phosphatase enzyme was induced in
95 response to P_i deficiency (15) (16). When extracellular P_i is abundant, *C. watsonii* employs the
96 constitutively expressed phosphate inorganic transport (Pit) system to import phosphorus into
97 the cell (15). Under P_i limiting conditions, a high-affinity phosphate-specific transport (Pst)
98 system, which uses ATP-mediated transport, is activated, and the high-affinity phosphate-
99 binding protein (PstS) is upregulated to enhance P_i uptake (16) (17). Comparative genome
100 analysis of six unicellular *C. watsonii* strains belonging to the two morphological phenotypes
101 (small and large cells) revealed a variation in the copy number of genes involved in the transport
102 and use of P_i (6). Whole-genome transcription analysis of *C. watsonii* cultures showed that
103 47.4% of the genes exhibited a diel expression pattern (18). In P_i -depleted cultures, the *pstS*
104 gene also displayed a diel expression pattern (16), indicating that adaptive mechanisms to cope
105 with P_i scarcity might follow diel regulation, likely by the circadian KaiABC clock (19).

106 The results summarized above point to results specific to *C. watsonii*, while a comprehensive
107 comparative overview of the genetic potential of the genus *Crocospaera* to cope with P_i
108 limitation is lacking. Here, we present a dual approach to the genetic and physiological response
109 to P_i limitation. First, to compare the genetic potential of the different *Crocospaera* strains,
110 we conducted a functional genomics analysis of P_i depletion-responsive genes across eight
111 *Crocospaera* genomes, including the six known *C. watsonii* strains and the coastal strains *C.*
112 *subtropica* and *C. chwakensis*. In each genome, we identified all genes involved in P_i uptake,
113 the hydrolysis of dissolved organic phosphorus (DOP), and the perception and regulation of
114 gene expression in response to P_i limitation. Second, we analyzed the expression of these genes

115 during P_i depletion in cultures of *C. watsonii* 8501. We also monitored the physiological
116 parameters of cells in conditions of P_i depletion, as well as during a recovery phase in which
117 DOP was provided to the P_i-depleted cultures.

118

119 **Experimental procedures**

120 **Strain and growth conditions**

121 *Crocospaera watsonii* strain WH8501, isolated in the western tropical South Atlantic Ocean,
122 was grown under obligate diazotrophy in a YBCII culture medium (20), which we slightly
123 modified to make sure the medium was devoid of any source of N (Fe-NH₄-citrate was replaced
124 with Fe-citrate). Cultures were kept at 27°C under a 12:12h dark:light cycle at 600 μmol
125 photons.m⁻².s⁻¹ to ensure light-saturated growth. The growth medium was prepared from aged
126 Mediterranean Sea water, collected at the Microbial Observatory Laboratoire Arago (MOLA)
127 station (at 19 miles off the coast, 42°27.200' N – 03°32.600' E, 500m depth, salinity 38). The
128 collected water was stored for at least 8 weeks in the dark at 20°C, filtered through 1 and 0.22μm
129 Whatman filters, and autoclaved before use. Before the experiment, we analysed the bacterial
130 contamination in the strain. Three strains of heterotrophic bacteria were identified:
131 *Nitratireductor aquibiodomus*, *Qipengyuania goetbuli*, and *Oceaniradius stylonematis*.
132 Bacterial contamination was then monitored during the experiments by flow cytometry with
133 Sybr Green staining (see below). The bacterial contamination represented between 3.63 ±
134 1.23% and 7.7 ± 2.48% of the total biomass considering a carbon content of 4 or 8.9 fmol C.cell⁻¹
135 as estimated in (21).

136 **Experimental design**

137 A phosphate-replete culture (grown with 50 μmol L⁻¹ of KH₂PO₄) was grown exponentially to
138 serve as inoculum for all the experiment replicates. This culture, which reached an exponential

139 growth rate of 0.26 d^{-1} ($R^2 = 0.95$), was then filtered and transferred into fresh medium to
140 prevent nutrient limitation and to allow a biomass build-up to the desired level. Once the
141 biomass reached $10^7 \text{ cells mL}^{-1}$, the culture was filtered again and equally resuspended in 6
142 flasks containing fresh culture medium devoid of P_i , aiming at an initial concentration around
143 $3.5 \cdot 10^6 \text{ cells mL}^{-1}$ in each flask. Due to the total estimated volume required for this experiment
144 and the size limitations of the culture flasks, each replicate consisted of two flasks, each
145 containing 2.5 L of P_i -depleted culture. The six cultures were maintained under P_i -depletion for
146 a total of 9 days. All culture replicates were started simultaneously and monitored daily for cell
147 abundance to verify that all population dynamics were equivalent. To ensure that the P_i
148 remaining after dilution had been consumed and cells were experiencing P_i starvation, we
149 waited for five days and initiated a high frequency monitoring from the 6th day (labelled as Day
150 1 of monitoring on the figures) after the transfer to the P_i -depleted medium. In total, cultures
151 were monitored for 4 continuous days as follows: sampling started at the dark-light transition
152 (L0) and was then performed every 3h, at L3, L6, L9, D0, D3, D6, D9, where L and D stand
153 for light and dark, respectively. This sampling was performed in the first triplicate for the first
154 3 days; after the light-dark transition of the third day (Day 3, D0), the first replicate was nearly
155 drained and sampling continued in the second triplicate.

156 Following the 9-day period in P_i -depleted conditions, a recovery phase was initiated in the
157 remaining (2nd) triplicate. The cultures were diluted in fresh, 2X (twice concentrated) YBCII
158 medium devoid of phosphate and containing a mix of dissolved organic phosphorus (DOP),
159 with a final concentration of $50 \mu\text{mol P L}^{-1}$ in the culture medium. We used an equal proportion
160 of adenosine diphosphate, alpha glycerophosphate, nitrophenyl phosphate, and glucose 6
161 phosphate, each at a final concentration of $12.5 \mu\text{mol P L}^{-1}$ in the medium. To proceed with the
162 DOP addition, 1 L of each of the remaining 3 replicates was sampled and transferred into an
163 autoclaved, 3L erlenmeyer containing 750 mL of DOP enriched medium. After the DOP

164 addition, the cultures were let to recover for 3 days and then monitored again at high frequency
165 for 2 days.

166 **Analytical methods**

- 167 • Cell size and abundance

168 *Crocospaera* cell abundance was estimated using a Coulter Cytoflex (Beckman) flow
169 cytometer by auto-fluorescent cell detection. Samples were taken for cell count at daily intervals
170 before (during the P-replete growth phase) and after inoculation in a P_i -depleted medium, and
171 then every 3h during the high-frequency monitoring. The samples were fixed with
172 glutaraldehyde (final concentration 0.5%) and conserved at -80°C until analysis. The
173 contamination of the culture by heterotrophic bacteria was also verified by flow cytometry, in
174 a second procedure after staining with SyberGreen. Thus, two acquisition procedures were
175 applied based on the size and abundance differences between *Crocospaera* and the
176 heterotrophic bacteria. The growth rate was derived from cell counts by exponential regression
177 of the abundance counts. The equivalent spherical diameter (ESD, μm) of each *Crocospaera*
178 cell was estimated by comparing the total forward scatter diffusion (the area under the FWS
179 pulse shape) of the cells and that of manufactured Silica beads (known diameter of 1.05, 1.97,
180 3.93, $3.93\mu\text{m}$; silica microsphere, Bangs Laboratories $\text{\textcircled{R}}$) every day of analysis. The particle-
181 by-particle size data were extracted and analysed using FlowJo and R softwares. The biovolume
182 (BV, μm^3) was estimated with the following relation: $BV = \frac{\pi}{6} * ESD^3$ (Sun, 2003), with ESD
183 the equivalent spherical diameter, and considering that *Crocospaera* cells are spherical (5).

- 184 • Alkaline phosphatase activity

185 Alkaline phosphatase activity (APA) was monitored 3h after each light-dark transition: at L3
186 and D3, and was quantified using the fluorogenic substrate 4-Methylumbelliferone-Phosphate
187 (MUF-P) (22) at a final concentration of $125 \mu\text{mol L}^{-1}$. Samples ($210\mu\text{L}$) were incubated in

188 triplicate in black microplates at the culture temperature for 2 h. Control blanks were prepared
189 from Milli-Q water with added MUF-P substrate. The fluorescence intensity was measured
190 using a Perkin Elmer Victor3 Plate Reader fluorometer with an excitation wavelength of 365nm
191 and an emission wavelength of 450 nm. Fluorescence readings were done at t_0 (time of MUF-
192 P addition), $t_0 + 30$ min, $t_0 + 1$ h, and $t_0 + 2$ h. The increases in fluorescence, confirmed to be
193 linear during the incubations, were transformed into enzyme activity rates using a standard
194 curve obtained from a MUF solution with concentrations ranging from 0 to 100 $\mu\text{mol.L}^{-1}$.

195 • Particulate and dissolved nutrients

196 Samples for biochemical analyses were taken during the high-frequency monitoring phase. The
197 particulate organic matter was determined every 6h, at L0, L6, D0, and D6. In each culture, two
198 samples of 6.27mL were collected independently, one to analyze particulate organic carbon
199 (POC) and nitrogen (PON) by complete combustion and the other for PON and particulate
200 organic phosphorus (POP) quantification by wet oxidation. As PON was quantified with two
201 distinct techniques, we differentiated PON_c obtained by combustion from PON_{oxi} obtained
202 through wet oxidation analysis. Culture samples were filtered on pre-combusted (450°C - 4h)
203 GF/C filters (nominal pore size 1.2 μm , Whatman). The filters were then dried and stored at
204 60°C before analysis. POC and PON_c filters were exposed to HCl fumes (4h) before analysis
205 using a CHNS elemental Analyzer (Thermo Fisher Scientific) calibrated with acetanilide (23).
206 PON_{oxi} and POP were estimated with a Segmented flux analyzer (Skalar), using the wet
207 oxidation technique according to (24). C, N, and P cell contents (fmol cell^{-1}) were deduced
208 knowing the precise volume of the sample and the cell abundance. Because the two analytic
209 techniques yielded different estimations of PON, we did not derive the biomass C:N:P
210 stoichiometry. Instead, we expressed the C:N (deduced from the combustion analysis; mol:mol)
211 and the N:P (deduced from the wet oxidation procedure; mol:mol) ratios separately.

212 Dissolved nutrients were sampled at L0 and D0 in each culture and conserved at -20°C before
213 analysis. 30mL-samples were filtered on two GF/F combusted (450°C - 4h) filters (nominal
214 pore size <0.5 , Whatman). Filtrates of 7mL were used to quantify dissolved inorganic nitrogen
215 (DIN) and phosphorus (DIP) according to Aminot et al. (2007) with a Segmented flux analyzer
216 (Skalar). Standard solutions of NO_3^- between 0 and $20 \mu\text{mol.L}^{-1}$ and blanks were prepared at
217 the same salinity as the sample. Total dissolved nitrogen (TDN) and phosphorus (TDP) were
218 analyzed with 10 mL of filtrate, according to the wet oxidation technique of Valderrama (1981),
219 with a Segmented flux analyzer (Skalar). Duplicates of $500\mu\text{L}$ filtrate with $125 \mu\text{L}$ of reagent
220 were used to quantify ammonium (NH_4^+). The fluorometric measure was realized 4 hours after
221 sampling, according to (25) using a Denovix fluorometer with an excitation wavelength around
222 375nm and an emission wavelength between 435 and 485 nm . A calibration curve was
223 constructed using concentrations ranging from 0 to $5 \mu\text{mol L}^{-1}$ in a NaCl solution at the same
224 salinity as the sample.

225 **RNA sampling and preparation, reverse transcription, and quantitative Real-Time-PCR**

226 Every 3h, 60 mL samples were collected and filtered through a $3\mu\text{m}$ pore-size polycarbonate
227 membrane filter. The cells were resuspended in ($0.2\mu\text{m}$ filtered and autoclaved) seawater, and
228 centrifuged at 5000rpm for 15min. The pellet was transferred in 5mL RNA later, immediately
229 frozen in liquid nitrogen, and stored at -80°C until analysis. All measurements were carried out
230 in duplicate. RNAs were extracted using the Qiagen RNA-extraction kit following the
231 manufacturer's instructions. An extra TURBO DNase (Invitrogen) digestion step was
232 performed to eliminate the contaminating DNA. The RNA quality was assessed by a tape
233 station system (Agilent). RNAs were quantified spectrophotometrically at 260 nm (NanoDrop
234 1000; Thermo Fisher Scientific). For cDNA synthesis, 200 ng total RNA and $0.5 \mu\text{g}$ random
235 primers (Promega) were used with the GoScript™ Reverse transcriptase (Promega) according

236 to the manufacturer's instructions. Quantitative real-time PCR (qPCR) analyses were performed
237 on a CFX96 Real-Time System (Bio-Rad). The reaction volume was 15 μ L and the final
238 concentration of each primer was 0.5 μ M. The qPCR cycling parameters were 98°C for 2 min,
239 followed by 45 cycles of 98°C for 5 s, and 59°C for 10 s. The only exception was the 5'ND
240 encoding gene, for which the melting temperature was 55°C. A final melting curve from 65°C
241 to 95°C was added to determine the specificity of the amplification. To determine the
242 amplification kinetics of each product, the fluorescence derived from the incorporation of
243 SYBR[®] Green Dye into the double-stranded PCR products was measured at the end of each
244 cycle using the SsoAdvanced Universal SYBR[®] Green Supermix 2X Kit (Bio-Rad, France).
245 The results were analyzed using Bio-Rad CFX Maestro software, version 1.1 (Bio-Rad,
246 France). The RNA 16S gene was used as a reference for normalization. The amplification
247 efficiencies of each primer pair were 80 to 100%. All measurements were carried out in
248 triplicate, a biological duplicate was performed for each point, and standard variations were
249 calculated for each measure. The primers used in this study are listed in **Supporting**
250 **information Table S1.**

251

252 **Bioinformatics analysis**

253 **Datasets**

254 The genome data of 8 *Crocospaera* strains available in September 2023 were downloaded
255 from the NCBI ftp site (<ftp://ftp.ncbi.nih.gov/genomes/>) and constituted the primary data source.
256 This data source includes full genomes in the highest levels of assembly (complete genome,
257 scaffold, or Contig), their RefSeq category (representative genome or none) as well as their
258 annotation features (**Supporting information Table S2, Sheet 1**). Note that *Crocospaera*
259 species DT_26, ALOHA_ZT_9, and MO_202 were excluded from our set of genomes because
260 these genomes are derived from metagenome assemblies. Cell-size features of *C. watsonii*

261 (small and large) were provided by the literature (6). Hidden Markov Models (HMMs) of
262 protein family profiles (Pfam version 35.0, April 2023) and Pgap (version 4, April 2023) were
263 downloaded from <ftp.ebi.ac.uk/pub/databases/Pfam/releases/> and
264 <ftp.ncbi.nlm.nih.gov/hmm/4.0/> ftp sites, respectively. Seed proteins (52 in total) used as
265 references (retrieved from the Uniprot database, www.uniprot.org) in this study are described
266 in **Supporting information Table S2, Sheet 2**. Proteins from cyanobacteria were used as
267 probes when available; otherwise, proteins from *E. coli* were used as alternatives.

268 **Functional domain search for orthologs identification**

269 HMMER package (26) and HMM domain profiles were first used to establish the list of seed
270 functional domains associated with reference seed proteins as well as their protein domain
271 organizations (or domain patterns) (**Supporting information Table S2, Sheet 2**). Alignments
272 with scores higher than the Pfam/Pgap trusted thresholds were considered significant seed
273 domains. This led to 76 reference seed domains from Pfam or Pgap domain databases
274 (**Supporting information Table S2, Sheet 3**). HMMER3 (26) and self-written Perl scripts
275 were then used to search for protein orthologs (with seed domains) in the set of *Crocospaera*
276 genomes. For each reference protein, the presence of one or more seed domains was a requisite
277 to identify putative orthologs. As described above, alignments with a score higher than the
278 Pfam/Pgap thrust thresholds were also considered significant and in the case of overlapping
279 domains, the longest ones with the best E-values were chosen. Putative orthologs of each seed
280 protein were subsequently analyzed with the same software to determine their domain patterns
281 with the potential presence of additional functional domains. Orthologs were then selected for
282 the strict presence of seed domains (i.e., in the right order and without additional domain), and
283 thus, led to the set of Hmm-homologs. To increase the sensitivity of the identification of
284 orthologs, a Blast (27) analysis search was performed using all reference seed proteins as
285 queries and an E-value threshold of 10^{-5} . Blast alignments with a MinLrap [Alignment size /

286 Minimum size (Query, Subject)] ≥ 0.8 and MaxLrap [Alignment size / Maximum size (Query,
287 Subject)] ≥ 0.8 were considered as significant and constituted the set of Blast-orthologs.
288 Hmm-homolog and Blast-homolog sets were finally combined to yield the final set of orthologs
289 for each reference protein. For comparative analysis, reference proteins with identical Pfam
290 domain patterns were considered identical seed proteins and then grouped as a unique reference
291 for analysis. This was the case for PhnE, PstA, PstC, PtxC, UgpA, and UgpE [leading to PhnE-
292 PstA-PstC-PtxC-UgpA-UgpE]; PhnC, PstB, PtxA, and PhnK [PhnC-PstB-PtxA-PhnK]; GppA
293 and ppX [GppA-ppX]; PhnD and PtxB [PhnD-PtxB]; and PstS and SphX [PstS-SphX].
294 To further analyze the presence or absence of several key genes involved within the four
295 systems known to be devoted to Pi limitation (Phosphate, Pst system; Phosphite, Ptx system;
296 Phosphonate, Phn system; and Glycerol, Ugp system), tBlastN analyses were additionally
297 performed. For that purpose, the corresponding seed proteins (associated to their localization:
298 periplasmic, inner membrane or cytoplasmic) of each system were compared against our dataset
299 of nucleotide genomic sequences with the E-value threshold was set to 10^{-5} for significant
300 alignments and considering the best hit as the most likely ortholog.

301

302 **Results**

303 [Functional genomics survey of Pi-related genes in *Crocospaera* genomes](#)

304 To evaluate the genetic capabilities of various *Crocospaera* strains in adapting to phosphate
305 (P_i) deficiency, a comprehensive search for homologs of proteins associated with transcriptional
306 regulation in response to P_i deficiency, phosphate import, and dissolved organic phosphorus
307 (DOP) hydrolysis was conducted. To achieve this, protein functional domain analysis,
308 supplemented with BLAST search were performed for each category of proteins as described
309 in the Experimental Procedures section. The findings for each functional category are outlined
310 in the sections below and **Supporting information Table S2, Sheet 4**.

311 Signal transduction and gene regulation

312 Genes encoding orthologs to the histidine kinase sensor PhoR and the response regulator PhoB
313 were detected in the genomes of the 8 analyzed *Crocospaera* strains, suggesting that this two-
314 component system (TCS) might, as in other bacteria, be the primary trigger of the P_i limitation
315 response (**Figure 1, Supporting information Table S2, Sheet 4**). The activity of the
316 PhoR/PhoB system is controlled according to the concentration of phosphate in the
317 environment. Under conditions where P_i is abundant, PhoU is essential for the
318 dephosphorylation of PhoB (28) and plays a role in negatively regulating both the activity and
319 the quantity of the Pst transporter to prevent excessive P_i uptake (29). This regulatory
320 mechanism might be conserved in *Crocospaera*, as an ortholog of the *phoU* gene was found
321 in all the *Crocospaera* genomes studied (**Figure 1, v**).

322 In the marine cyanobacterium *Synechococcus sp.* WH8102, the regulation of several P_i-related
323 genes involves a transcriptional regulator from the cAMP receptor protein (CRP) family, known
324 as PtrA, that acts downstream from the PhoBR system (30). At least one copy of orthologs to
325 *ptrA* was also found in all the *Crocospaera* genomes (**Figure 1, Supporting information**
326 **Table S2, Sheet 4**). Furthermore, a search for orthologs of the Psp1 protein from
327 *Prochlorococcus marinus* WH8102, predicted to be part of the CRP family, revealed the
328 presence of several copies of *psp1* genes in the *Crocospaera* genomes (**Figure 1**). Altogether,
329 these data indicate that CRP-like regulators probably have a significant role in coordinating the
330 response to P_i stress in this genus.

331 Phosphorus uptake

332 Gram-negative bacteria can internalize P_i via non-specific porin channels in the outer
333 membrane, facilitating the passive diffusion of small hydrophilic molecules. As an example,

334 the major outer membrane protein Som in *Synechococcus sp. PCC 7942*, is involved in the
335 uptake of these small molecules (31). In *Crocospaera*, the P_i uptake through the outer
336 membrane may also be achieved by the porin Som, as several copies of putative Som-encoding
337 genes were found in all the *Crocospaera* genomes studied (**Figure 1, Supporting**
338 **information Table S2, Sheet 4**). Those *som* genes are located close to *phoU* and *phoR* genes,
339 further suggesting a role of the Som porin in response to P_i stress. In *E. coli*, the porin PhoE,
340 which is part of the Pho regulon, facilitates the uptake of P_i across the outer membrane (32).
341 No PhoE ortholog was identified in the protein database of the *Crocospaera* strains studied
342 (**Figure 1, Supporting information Table S2, Sheet 4**), suggesting that a *phoE* gene is
343 unlikely to exist in this cyanobacterial genus.

344 To identify proteins that may facilitate P_i uptake across the cell inner membrane, we searched
345 for orthologs of the Pit system, which facilitates P_i entry under non-limiting conditions, and the
346 Pst system, which is activated under low P_i concentrations (15). Orthologs of the Pit protein
347 were found in the protein database of *C. watsonii* strains, but intriguingly, not in *C. subtropica*
348 and *C. chwakensis*. The absence of Pit orthologs is puzzling; given their coastal habitats, these
349 strains are unlikely to consistently face phosphorus limitation so we expected to find orthologs
350 of the low-affinity transport system Pit. Whether they utilize an alternative system for
351 constitutive P_i uptake therefore remains to be investigated. The Pst system is an ATP-binding
352 cassette (ABC) transporter comprising three essential units: PstC, PstA, and PstB. These are
353 encoded by the *pstSCAB* gene operon, which belongs to the Pho regulon. PstS, a periplasmic P_i
354 binding protein, delivers P_i to the transmembrane proteins PstC and PstA. PstB, a cytosolic
355 ATPase, uses ATP hydrolysis to import P_i into the cytoplasm (10). In cyanobacteria, a PstS
356 homolog, designated SphX, belongs to the phosphate-binding protein family and delivers
357 periplasmic P_i to the ABC transporter (33).

358 In addition to P_i , phosphites, phosphonates, and glycerol-phosphate can be used as sources of
359 phosphorus by bacteria. The uptake of these molecules through the inner membrane is achieved
360 by ABC transporters which belong to the same family as the Pst system. Phosphite is
361 incorporated through the Ptx system, phosphonate through the Phn system, and glycerol-
362 phosphate through the Ugp system. Each subunit of a given transporter shares the same
363 functional domain signature with its orthologs in the other systems, except for UgpC and UgpB,
364 which have distinctive functional domains (**Supporting information Table S2, Sheet 2**).
365 Consequently, using functional domains as a search tool to identify orthologs does not allow
366 the identification of subunits specific to each transporter. This analysis yields all potential
367 orthologs for each subunit group, as shown in the heatmap of **Figure 1, Supporting**
368 **information Table S2, Sheet 4**.

369 To specifically predict the presence of a complete set of genes for each transporter, we
370 completed our analysis using tBlastN. We considered the ortholog with the best hit for each
371 search as the most probable ortholog. The results indicate that all eight *Crocospaera* possess
372 a complete set of genes for the Pst system (**Figure 2 and Supporting information Table S2,**
373 **Sheet 5**). It should be noted, however, that in the case of *C. watsonii* WH8501, the *pstA* gene
374 is considered a pseudogene in NCBI database, which results in the absence of the corresponding
375 protein in the Refseq database. Therefore, the *pstA* gene cannot be retrieved from WH 8501
376 genome. The annotated pseudogene may be due to sequencing errors which may have
377 interrupted the open reading frame of this gene. Alongside the Pst system, the gene *phoH*, which
378 encodes a putative ATPase, is found in the Pho regulon of bacteria, although its exact function
379 remains unclear (34). Orthologs of PhoH were found in all *Crocospaera* genomes, suggesting
380 that this protein may play a role in adaptation to P_i limitation (**Figure 1**).

381 Gene orthologs encoding all the subunits of an Ugp transport system were identified in all the
382 *Crocospaera* genomes, suggesting that all eight strains may be capable of internalizing
383 phosphoglycerol (**Figure 2 and Supporting information Table S2, Sheet 5**). In contrast to the
384 Pst and Ugp systems, only the genomes of *C. subtropica* and *C. chwakensis* possess a complete
385 set of genes encoding all the subunits of the Ptx and Phn transporters (**Figure 2 and Supporting
386 information Table S2, Sheet 5**). Taken together, these genome analyses suggest that all
387 *Crocospaera* strains may be able to use phosphate and glycerol-phosphate. A discrepancy is
388 found within the genus regarding the use of phosphites and phosphonates, with the six *C.*
389 *watsonii* strains being likely unable to uptake them.

390 DOP hydrolysis

391 We carried out an extensive analysis in search of a wide variety of genes known to encode
392 enzymes capable of generating phosphate from various substrates, such as phosphoesters
393 (alkaline and acid phosphatases), polyphosphates (polyphosphatases), pyrophosphate inorganic
394 pyrophosphatase), and nucleotides (nucleotidases) (**Supporting information Table S2, Sheet
395 2**). Of all the alkaline phosphatases known in bacteria, only the *phoX* gene has been identified
396 in all the *Crocospaera* genomes. No ortholog to the *phoD* gene was found in the *C. watsonii*
397 WH8501, WH8502, and WH0401 genomes. The *phoV* gene was not detected in the *C. watsonii*
398 WH8502 genome and no ortholog to *phoA* was identified in *C. watsonii* WH8501.
399 Consequently, all *Crocospaera* strains are potentially able to hydrolyze DOP since their
400 genomes contain at least one gene encoding a typical alkaline phosphatase (**Figure 1,
401 Supporting information Table S2, Sheet 4**). In addition, all their genomes contain an
402 ortholog of the *dedA* gene encoding an alkaline phosphatase-like enzyme.

403 The use of inorganic pyrophosphate as a source of phosphate is probably limited to the *C.*
404 *subtropica* and *C. chwakensis* strains since an ortholog to the *ppA* gene encoding a

405 pyrophosphatase was only found in their respective genomes. Conversely, all strains might be
406 able to hydrolyze polyphosphates since at least one ortholog encoding a polyphosphatase (PpX
407 or GppA) was found in their genome. In addition, the eight *Crocospaera* strains might
408 synthesize polyphosphate reserves, as suggested by the presence of the *ppK* gene potentially
409 encoding a polyphosphate polymerase catalyzing polyphosphate formation from ATP.

410 Three nucleoases (NucH, SurE, and UshA) were identified in our study. While a SurE ortholog
411 was identified in all the genomes analyzed, only one UshA ortholog was identified in *C.*
412 *chwakensis* and the NucH gene was absent in all 8 genomes (**Figure 1, Supporting**
413 **information Table S2, Sheet 4**). The SurE 5' nucleotidase could be used for phosphate
414 recycling in the *Crocospaera* genus. It is worth noting that this gene is annotated as *phoA* in
415 some *Crocospaera* genomes, and this annotation error may mislead the interpretation of
416 functional measurements of phosphatase alkaline activities (see the Discussion section). Our
417 results also indicate that the genus *Crocospaera* could use phosphoglycerol as a source of
418 phosphate since orthologs to the *glpQ* and *ugpQ* genes encoding glycerol-phosphodiesterases
419 are present in the 8 genomes analysed. The ability to use phosphonates is likely restricted to *C.*
420 *chwakensis* as a complete set of genes for hydrolysis of these compounds (*phnGHIJM*) was
421 only found in its genome.

422 Interestingly, although only one strain of *Crocospaera* seems to have a phosphite entry system
423 (as mentioned above), the *ptxD* gene responsible for phosphite utilization was identified in all
424 8 genomes analyzed. This point raises an intriguing question: did the evolution of phosphite
425 use occur after the loss of genes encoding transporters in most strains, or are these genomes
426 currently acquiring these genes?

427 Other P_i-stress-responsive genes

428 Substituting phospholipids with sulfolipids is a strategy cyanobacteria may use to cope with P_i
429 scarcity (35). The presence of orthologs to the *sqdB* and *sqdX* genes, which encode two essential
430 synthases required for glyceroglycolipid synthesis, in all *Crocospaera* genomes (**Figure 1,**
431 **Supporting information Table S2, Sheet 4.**) suggests that this adaptive strategy might be
432 conserved within this genus.

433 Arsenate is a toxic substance coincidentally internalized by the P_i transporters due to its
434 similarity to P_i. As a result, inducing arsenate-reduction activities is part of the adaptive
435 responses to P_i limitation (36). The eight *Crocospaera* strains appear to be able to detect the
436 presence of arsenate, as their genomes contain an ortholog of the *arsR* gene, which encodes the
437 specific transcriptional regulator for genes encoding the arsenate reductase ArsC and the efflux
438 pump ArsB. Although the *arsC* gene is present in all *Crocospaera* genomes, *arsB* is absent in
439 the *C. watsonii* WH0401 (**Figure 1, Supporting information Table S2, Sheet 4.**). Arsenate
440 reduction might be the unique strategy to cope with its toxicity in this strain.

441 The relationship between morphotype and gene conservation was examined using three groups:
442 the *C. watsonii* small-cell strains (WH0401, WH8501, and WH8502), the *C. watsonii* large-cell
443 strains (WH0003, WH0005, and WH0402), and the ancient *Cyanothece* spp., newly classified
444 within the *Crocospaera* genus as *C. subtropica* and *C. chwakensis*. The gene encoding the
445 low-affinity P_i transporter, *pit*, was identified as an ortholog in the *C. watsonii* but not in the
446 new *Crocospaera* strains. Conversely, the new *Crocospaera* strains were the only ones to
447 possess genes encoding the phosphonate transporter (*phnGHIJ*), inorganic pyrophosphatase
448 (*ppA*), and 5'-nucleotidase (*ushA*) (**Figure 3, Supporting information Table S2, Sheet 5,6.**)
449 Overall, the percentage of total orthologs was lowest in the small-cell strains compared to the
450 other two groups. For example, the small-cell strains lacked orthologs for the potential alkaline
451 phosphatase (AP) gene *phoD*, while more sequences encoding AP (*phoA*, *phoD*, *phoX*, and

452 *pafA/phoV*) were found in the large-cell and new *Crocospaera* strains (**Figure 3, Supporting**
453 **information Table S2, Sheet 5,6**).

454 Diel expression of genes involved in P_i-depleted and DOP-recovery conditions

455 To investigate the genetic response of *Crocospaera* to phosphorus-depleted (P_i-depleted) and
456 DOP recovery conditions, we analyzed the transcription of P_i-related genes every 3 hours over
457 4 days under P_i-depletion and then over 2 more days after the same cultures were supplied with
458 DOP.

459 The expression of *ptrA*, which encodes a potential regulator in response to P_i limitation, was
460 low during the Pi depletion phase and followed a daily cycle with peaks during the light phase.
461 Specifically, the peaks occurred at L9 on Day 2 and L6 on Day 4 (**Figure 4A**). 3 days after
462 DOP addition, *ptrA* expression was three times lower than the first sampling point (L0, Day 1)
463 of the P_i-depleted phase (**Figure 4A**).

464 Given that genes encoding P_i transporters are organized in clusters, suggesting a possible
465 operonic organization, we chose to analyze the expression of the first gene, encoding the
466 binding protein, in each cluster as a representative of the entire gene cluster. The genes encoding
467 the binding protein of the high-affinity P_i transporter (PstS) followed a daily expression cycle,
468 peaking at the light-dark transition (D0). The *pstS*-homolog *sphX* gene peaked three hours
469 before the light-dark transition (L9) in the P_i-depleted phase (**Figure 4B**). The gene encoding
470 the glycerol-phosphate molecule binding protein (UgpC) showed a low but cyclic expression,
471 with a higher expression during the light phase than the dark phase (**Figure 4B**). The porin
472 Som-encoding gene displayed the same expression profile as *pstS*. During the DOP-recovery
473 phase, the expression peaks of *som*, *pstS*, and *sphX* occurred at the same times as during the P_i-
474 depleted phase. However, the expressions of *pstS* and *sphX* were lower compared to the P_i-

475 depleted phase (four times lower on Day 8 for *sphX*, and on Days 8 and 9 for *pstS*), whereas
476 *ugpC* expression was ten times higher on Days 8 and 9 compared to Day 1 (**Figure 4B**).

477 Genes potentially encoding enzymes required for P_i scavenging were expressed globally at a
478 low level (**Figure 4C and Supporting information Figure S1**). During the P_i-depleted phase,
479 the genes encoding the glycerophosphoesterase UgpQ and the 5'-nucleotidase (5'ND) showed
480 oscillatory patterns (**Figure 4C**). UgpQ transcription peaks in the light phase were over ten
481 times higher than the initial point on Days 2 and 3 (**Figure 4C**). The expression of the 5'ND
482 encoding gene peaked during both light and dark phases and increased over tenfold during the
483 DOP-recovery phase (**Figure 4C**). Other genes encoding enzymes, such as the potential
484 5'nucleotidase SurE, a metallophosphoesterase, the alkaline phosphatase-like (DedA)
485 (**Supporting information Figure S1**), and the alkaline phosphatase PhoX, were lowly
486 expressed throughout the experiment (data not shown). In conclusion, the expression of genes
487 potentially encoding a high-affinity P_i transporter exhibited diel variations during both the P_i
488 depletion and DOP recovery phases. In contrast, genes predicted to encode DOP-hydrolyzing
489 enzymes were expressed at low levels and displayed different patterns between the two growth
490 phases.

491 [Expression of circadian clock genes](#)

492 The observed daily cyclical gene expression may be driven by circadian control exerted by an
493 internal clock. Initially identified in the unicellular cyanobacterium *Synechococcus elongatus*
494 PCC7942 (37), the circadian clock is largely conserved within cyanobacteria (38). But, to our
495 knowledge, the circadian clock has not yet been studied in *C. watsonii* WH8501. To investigate
496 whether the cyclic expression of the genes studied is linked to a circadian control, we searched
497 for homologs of the *kaiA*, *kaiB*, and *kaiC* genes, which constitute the *Synechococcus* clock, as

498 well as the *rpaA* gene, which encodes a transcriptional regulator that transduces the control
499 generated by the clock (39).

500 Homologs of the *kaiABC* genes were identified in the *C. watsonii* WH8501 genome, clustered
501 together (**Figure 5A**). In *Synechococcus*, the *kaiB* and *kaiC* genes form an operon, and all three
502 *kai* genes exhibit circadian expression (39). In the *C. watsonii* WH8501 genome, the *kaiA* and
503 *kaiB* genes are contiguous, suggesting they belong to the same transcriptional unit. Analysis of
504 the transcription of these three genes under the experimental conditions described above reveals
505 an intriguing profile. While the *kaiB* and *kaiC* genes showed circadian expression with a
506 transcriptional peak at light-dark transition, the expression of the *kaiA* gene did not appear to
507 be circadian and followed a different profile from that of *kaiB* (**Figure 5B, C, D**). These findings
508 support the hypothesis that the clock controls gene expression in *C. watsonii* WH8501.
509 However, they also suggest that the functioning of this clock may differ from that in
510 *Synechococcus*, calling for further investigation. Additionally, the transcription of the *rpaA*
511 gene was cyclic, with peak activity during the night phase (**Figure 5D**), consistent with its
512 predicted role in the output system acting downstream of the clock.

513 Population dynamics

514 We followed the cell abundance during P starvation and DOP recovery by flow cytometry to
515 compare the changes in population dynamics and quantify the growth rates. Upon transfer of
516 the exponentially growing cultures to a P_i-depleted medium, the initial cell concentration in the
517 P_i-depleted replicates was $3.49 \pm 0.22 \cdot 10^6$ cells mL⁻¹ (n=6). A transient increase in cell
518 abundance was visible in all cultures, which grew at a rate of 0.23 ± 0.03 d⁻¹ on average (n=6
519 replicates with 5 time-points) over the first four days (days -4 to 0, **Supporting information**
520 **Figure S2**). This rate is slightly lower than the rate observed in the seed culture grown on P_i
521 (0.26 d⁻¹) but it was also estimated in denser cultures, which most probably experienced a

522 slightly lower irradiance compared to the seed culture. In that respect, the initial growth rate in
523 the P_i -depleted phase was comparable to that observed in the seed culture grown with P_i . In
524 contrast, the exponential phase appeared much shorter in time. An inflection in the temporal
525 fluctuation of the cell abundance was visible from the 5th day into the P_i depleted phase (day
526 1); the biomass kept increasing for another couple of days, albeit at a slower pace, and reached
527 a plateau with an average cell abundance of $1.05 \cdot 10^7$ cells mL^{-1} in the 6 replicates (**Supporting**
528 **information Figures S2 and 6A**). Overall, in 8 days, the cell number tripled and cells divided
529 1.6 times on average, resulting in an average growth rate of $0.14 d^{-1}$ over the 8 first days of P_i
530 depletion. Cell abundance thereafter initiated a decrease from the 9th day into the P_i -depleted
531 phase (day 4) when the DOP-containing medium was added to the 3 remaining replicates. Cell
532 counts recorded on the 4th and 5th day following the DOP addition indicate that cells started
533 growing again (**Figure 6A**), at a rate of $\mu_{+DOP} = 0.31 \pm 0.01 \text{ day}^{-1}$ ($n=16$ for each replicate;
534 average from the three estimated rates) over the two days of monitoring. We do not consider
535 this rate very accurate as it derives from two consecutive days only and the doubling time at
536 this growth rate is more than two days. However, the consistency of the estimates between the
537 three replicates as well as the clear difference in population dynamics compared to the P_i -
538 depleted phase are solid proof for the good recovery of the strain and the use of (some, at least)
539 of the DOP compounds provided to re-initiate growth.

540 Under non-limiting nutrient conditions, cell size is known to follow a diel cycle of increase
541 between the end of the dark phase and the end of the light phase, and decrease during the dark
542 phase (40) (41). Under the present, transient conditions of P_i starvation, cell size kept oscillating
543 with a similar tendency to increase in the light and decrease in the dark. The timing of these
544 oscillations was very consistent between all replicates, albeit with diverging average sizes
545 during the P_i depletion. The average cell diameter was $2.79 \pm 0.07 \mu m$ ($n=92$). Without
546 sufficient size records under the initial, phosphate-replete growth, we cannot assess whether the

547 P_i depletion affected the average cell size. The measured values still fall within the ranges
548 usually observed for this strain (42) (41) (43). The corresponding biovolume was 11.94 ± 0.89 ,
549 11.60 ± 0.60 , and $10.70 \pm 0.62 \mu\text{m}^3 \text{ cell}^{-1}$, with an overall average of $11.41 \pm 0.88 \mu\text{m}^3 \text{ cell}^{-1}$
550 ($n=92$) (**Figure 6B, days 1 to 4**). On the fourth day following the refreshment of cultures into
551 the DOP-containing medium (days 8 and 9), the amplitude of diel oscillation in cell size had
552 doubled. The average cell diameter was 2.90 ± 0.10 ($n=16$), 2.74 ± 0.11 ($n=16$), and 2.66 ± 0.11
553 μm ($n=16$) in the three replicates, with an overall average of $2.77 \pm 0.14 \mu\text{m}$ ($n=48$). The
554 corresponding biovolume was then 12.86 ± 1.24 , 10.80 ± 1.25 , and $9.91 \pm 1.19 \mu\text{m}^3 \text{ cell}^{-1}$ in the
555 three replicates, with an overall average of $11.19 \pm 1.73 \mu\text{m}^3 \text{ cell}^{-1}$. This much wider fluctuation
556 in cell size at the diel scale suggests a recovery of carbon fixation, accumulation in the light,
557 and consumption in the dark.

558 In addition to the diel oscillation, a transient decrease in cell size also normally occurs around
559 the mid-light phase in nutrient-replete cultures, consequent to cell division (40, 41). In the
560 present experiment, no decrease in cell diameter can be observed around mid-light during the
561 P_i -depleted phase, while it becomes visible during the DOP recovery. This is another evidence
562 for the disruption of cell division towards the end of the P_i -depleted phase and for the recovery
563 of growth and cell division after cultures were provided with DOP. (**Supporting information**
564 **Figure S2**)

565 [Dissolved macronutrients and alkaline phosphatase activity](#)

566 We monitored dissolved N and P concentrations in the cultures and DOP hydrolytic activities
567 to track the consumption of nutrients, which also informs on growth efficiency. Nitrate (NO_3^-)
568 concentrations were close to zero ($0.36 \pm 0.28 \mu\text{mol N L}^{-1}$) during the whole experiment (**Table**
569 **1**) since the medium did not contain any added nitrate. Organic (DON) and total dissolved
570 nitrogen (TDN) levels were both higher during the DOP-recovery phase compared to the P_i -

571 depleted phase (19.10 ± 1.70 vs 9.19 ± 0.91 $\mu\text{mol N L}^{-1}$ for DON and 19.68 ± 1.74 vs $9.44 \pm$
572 0.91 $\mu\text{mol L}^{-1}$ for TDN; **Table1**). Most likely, N exudation processes were strongly reduced
573 under P_i depletion and restored during the recovery phase. The exuded DON in the recovery
574 phase may also be constituents of DOP hydrolytic enzymes.

575 During the P_i -depleted phase, the measured total dissolved P (TDP) in all cultures showed mean
576 concentrations as low as 0.21 ± 0.02 $\mu\text{mol P L}^{-1}$, with 0.03 ± 0.02 $\mu\text{mol P}_i \text{ L}^{-1}$ and 0.18 ± 0.03
577 $\mu\text{mol DOP L}^{-1}$ (**Table1**). Three days after the DOP addition (days 8 and 9), DOP concentrations
578 had dropped to a range between 0.15 and 1.17 $\mu\text{mol P L}^{-1}$ while phosphate levels were between
579 2.16 and 4.81 $\mu\text{mol P L}^{-1}$ on day 8 and showed a decreasing trend over the two days monitored
580 (**Table 1**). These results suggest that most of the DOP added was rapidly hydrolyzed and the
581 liberated P_i was mostly incorporated in cells. The alkaline phosphatase activity assay (APA)
582 was used to assess the production and activity of DOP-hydrolyzing enzymes. The expression
583 of alkaline phosphatases is part of the cell response to phosphate limitation in cyanobacteria
584 (44) (45) (46) (47), including diazotrophic strains (15) (14). The APA yielded rather low and
585 stable activities during the P_i -depleted phase, with an overall average recorded activity of 1.56
586 ± 0.79 $\text{fmol cell}^{-1} \text{ h}^{-1}$ ($n = 22$). Rates increased 3.15-fold during the DOP-recovery phase, with
587 an overall average of 4.90 ± 1.32 $\text{fmol cell}^{-1} \text{ h}^{-1}$ ($n = 12$) (**Table 1**).

588 **Particulate carbon, nitrogen, phosphorus, and C:N:P ratios**

589 The total *Crocospaera* C, N, P biomass and its stoichiometry were followed and normalized
590 by the population abundance to derive cellular contents. We consider all particulate C, N and P
591 to be part of the cells. Exuded EPS may also be collected on filters but we consider the
592 contribution of EPS to be very small in these thin, monocultures. During the four days
593 monitored in the P_i -depleted phase, the cellular carbon (POC) and nitrogen (PON) contents
594 fluctuated somewhat irregularly, without any evident diel pattern reproduced from one day to
595 the next (**Figure 7A, B, C**). The last record in replicate B, which stands as an outlier in this data

596 set, is not considered in the following. Although irregular, the variations in the carbon cell
597 contents remained in a rather conserved interval between 259 (163 if considering the first point
598 that also stands out of the general trend) and 434 fmol C cell⁻¹, with a very slight decreasing
599 trend of 8 fmol C lost per cell and day on average (**Figure 7A**). The cellular nitrogen content
600 (PON_c) also varied in a rather conserved range between 26 and 45 fmol N cell⁻¹, with a
601 decreasing trend in time of 1.89 fmol N lost per cell and day (**Figure 7C**). Carbon and nitrogen
602 acquisition occurred but could not completely compensate for the losses. Compared to the
603 steady, diel oscillations in the C and N contents reported in exponentially growing cultures (48)
604 (40) (41) (49), the more erratic, transient changes in the present data suggest that both the C
605 and N metabolism were partly impaired over those days. The resulting C:N ratio still showed
606 the diel oscillations known for this strain that result from the temporal decoupling of C and N
607 acquisitions. However, the increasing trend drifting far above the Redfield (1934) (50)
608 canonical reference (with values between 10 and 12 on the last day of the P_i-depleted phase)
609 reveals a skewed N stoichiometry: N incorporation was proportionally more impaired than C
610 fixation. Data also suggest that cells in one culture replicate tended to present higher C, N and
611 P contents than the other two (**Figure 7A-D**, blue curve). But cells were also somewhat bigger
612 in that replicate (**Figure 6B**); as a result, C and N content normalized by the biovolume showed
613 more similar values in all three replicates (**Supporting information Figure S3**). The cellular
614 P content fluctuated between 0.72 and 1.69 fmol P cell⁻¹, considering the last point of replicate
615 B as an outlier. The null derivative of this trend suggests that the average P content in cells
616 remained rather constant over the four days monitored in the P_i-depleted phase (**Figure 7D**).
617 The resulting mol:mol N:P ratio varied with no obvious diel trend, between 17.0 and 28.5, and
618 showed an average value of 22.9 ± 2.9 ($n = 47$) (**Figure 7F**). This average is markedly above
619 the Redfield reference, indicating that the cellular P content is particularly low with respect to
620 N. Altogether, these results suggest that under severe phosphate depletion, the P stoichiometry

621 strongly drops and the N stoichiometry is also reduced, while carbon acquisition seems
622 proportionately less affected.

623 During the recovery phase, the cellular carbon content fluctuated within a similar range as
624 during the P_i -depleted phase (**Figure 7A**). In contrast, the cellular N content showed much
625 wider and more regular oscillations, between a minimum level equivalent to that of the P_i -
626 depleted phase, and a 50% higher maximum (29 to 63 fmol N cell⁻¹; **Figure 7D**). As a result,
627 the C:N ratio in cells followed marked, diel oscillations around an average value of 8.8 (**Figure**
628 **7E**), which is lower than the average observed at the end of the P_i -depleted phase but still above
629 the Redfield value of 6.6. These fluctuations point to an increase in the carbon and nitrogen
630 fixation efficiencies compared to the P_i -depleted phase. Likewise, the particulate P content
631 shows notably higher levels in the recovery phase, with a 2.4-fold increase (**Figure 7D**).
632 Considering the first point of replicate A as an outlier, the average cellular P content was $2.6 \pm$
633 0.4 fmol P cell⁻¹ in the recovery phase, against 1.1 ± 0.2 in the P_i -depleted phase. These results
634 corroborate the strong decrease in DOP concentrations and point to an efficient DOP hydrolysis
635 and incorporation of the released P_i in cells. The corresponding N:P ratio thus dropped to values
636 in the range of 10.3 to 15.5, below the Redfield ratio, with an average of 13.0 ± 1.6 ($n = 24$)
637 (**Figure 7F**). Available records of the N:P composition in *C. watsonii* under nutrient-replete
638 conditions indicate a possible wide fluctuation of the cellular P content, with reports of N:P
639 ratios (mol:mol) from less than 5 (51) to over 30 (52). In a previous study conducted in P
640 replete conditions with P provided either as P_i or DOP, N:P ratios in the same *C. watsonii* strain
641 ranged between 7.9 and 9.8 (14). With over twofold higher N:P ratios observed in P_i -depleted
642 cells in the present study, the cell stoichiometry was imbalanced and shifted. The prolonged P_i
643 deficiency resulted in a far lower relative P content than P-replete conditions and we suspect
644 cells had reached their minimum P quota.

645

646 Discussion

647 The impact of nutrient limitation on nitrogen fixation in the open ocean is a widely studied
648 topic, given the significance of diazotrophs in the input of new nitrogen in the system. The
649 current literature provides several studies highlighting the role of P_i in the growth and nitrogen
650 fixation rates of filamentous cyanobacteria, such as *Trichodesmium* (53) (54) (55) (56) (57).
651 However, our understanding of how P_i influences the physiology of unicellular photosynthetic
652 diazotrophs, especially those in the *Crocospaera* genus, remains more limited, as does our
653 knowledge of how P_i availability might affect their growth. To address these questions, we
654 conducted a multidisciplinary study that included the functional analysis of six *Crocospaera*
655 genomes from three different species (*watsonii*, *chwakensis*, and *subtropica*). Additionally, we
656 analyzed the transcription of a wide range of genes involved in the response to P_i stress in *C.*
657 *watsonii*. Last, we monitored the growth of this cyanobacterium under P_i -depletion, tracked the
658 changes in its C, N and P composition, and assessed its ability to use alternative sources of P.

659 The estimated bacterial contamination of 3 to 7 % of the total biomass is rather low in such
660 long-term cultures; we can reasonably consider that the changes in the C:N:P composition of
661 the total biomass reflects that of *Crocospaera*. Besides, from a biogeochemical point of view,
662 all mass fluxes eventually derive from *Crocospaera*; the medium did not contain any source
663 of N (apart from the vitamins) so the contaminating bacteria can only feed on *Crocospaera* C
664 and N exudates. Also, due to the specificity of the genetic analysis, all gene expressions reported
665 here exclusively relate to *Crocospaera*.

666 We identified genes involved in P_i import, DOP utilization, perception of P_i limitation, and
667 regulation of P_i stimulus expression in the six analyzed genomes, noting some variations in the
668 composition of these genes (**Figure 1, Supporting information Table S2**). Regarding import,
669 all six strains contained a complete high-affinity P_i uptake system. Our analysis refined the

670 identification of these genes, correcting ambiguities caused by annotation errors. Notably, the
671 *pstA* gene, which encodes one of the two membrane subunits of this system, is absent from the
672 *C. watsonii* genome and is considered a pseudogene in NCBI. However, the literature
673 previously listed two copies of the gene in this strain [18]. Through tBlastn analysis, we
674 demonstrated that said *pstA* gene was mistakenly annotated as two separate small fragments in
675 the NCBI database but is actually a unique gene. We conclude that the eight *Crocospaera*
676 strains have a similar PstS ABC transporter (**Figure 2**). The low-affinity P_i permease PitA,
677 whose encoding gene was identified in *C. watsonii* WH8501, *C. watsonii* WH0002, and *C.*
678 *watsonii* WH0401, was also found in the protein dataset of four other *C. watsonii* strains (*C.*
679 *watsonii* WH8502, *C. watsonii* WH0402, *C. watsonii* WH0003, and *C. watsonii* WH0005),
680 suggesting it is well conserved in the *C. watsonii* representatives of the *Crocospaera* genus.
681 In contrast, no *pitA* ortholog was found in the genomes of *C. subtropica* and *C. chwakensis*.
682 Should PitA serve to facilitate P_i entry in *Crocospaera*, this activity might have been acquired
683 by, or maintained in, the *C. watsonii* strains only (**Figure 1**).

684 Genes encoding a complete phosphite and phosphonate transport system are absent in the
685 genomes of *C. watsonii* strains, but are present in *C. subtropica* and *C. chwakensis*, indicating
686 a possible adaptive speciation event. Given that phosphonates are produced, consumed and
687 therefore found in all marine waters, including oligotrophic regions (58), we wonder what
688 environmental conditions may have driven this divergence in their genomic content (**Figure 1,**
689 **Figure 2, Supporting information Table S2**). This is all the more puzzling as an inverse
690 relationship was highlighted between phosphonate catabolic genes and P_i availability across a
691 range of marine basins, suggesting that phosphonates are a source of phosphorus for the
692 bacterioplankton in oligotrophic areas (59). Future metagenomic surveys will be necessary to
693 determine whether the genes involved in phosphonate uptake and degradation are expressed
694 and functionally active in *C. subtropica* and *C. chwakensis*.

695 The analysis of the genes involved in DOP hydrolysis underscores the accuracy of domain-
696 search approach to achieve a rigorous functional annotation. For instance, a gene annotated as
697 *phoA* in the *C. watsonii* WH8501 genome suggested the presence of an alkaline phosphatase
698 (15). However, we did not find a *phoA* gene in this strain genome; our results reveal instead
699 that said gene encodes a 5' nucleotidase. Conversely, a *phoX* gene is present and conserved in
700 all the *Crocospaera* genomes studied. At least one other gene encoding an alkaline
701 phosphatase of another class (*phoA*, *phoD*, *phoV*, *dedA*) was also found for each genome. To
702 verify that the absence of a specific gene is not an artifact of our methodology, we additionally
703 performed a tBlastN analysis for these missing genes. Apart from the *pstA* gene previously
704 mentioned, our results confirmed the absence of all the genes that we did not find using the
705 domain approach (**Figure 1**).

706 Our data collectively suggest that genes related to DOP hydrolysis are present in *Crocospaera*
707 genomes but raise the question as for which enzyme(s) are actually operating. The next
708 challenge is to associate each gene with a specific DOP-scavenging activity. Biochemical
709 assays using the MUF-P reagent have demonstrated DOP hydrolytic activities in cultures of *C.*
710 *watsonii* grown with DOP supplementation (14) (17). Similarly, we observed comparable
711 activities when P_i-depleted cultures were shifted to the DOP-recovery phase (**Table 1**).
712 Although *phoX* transcript levels were low, we cannot dismiss the possibility that the measured
713 activity might be attributed to the PhoX enzyme. Under our experimental conditions, *phoX*
714 expression might have reached a steady-state level following the phase of P_i depletion. Also,
715 the transcription of genes encoding hydrolytic activities may be constrained in time. In their
716 experiment, Pereira and colleagues (17) observed a notable increase in APA in cultures upon
717 transfer to a P_i-depleted medium, which confirms that APA responds to P_i stress. In contrast,
718 APA was low in our cultures, but these measurements were taken after 5 days of P_i starvation.
719 In parallel, the monitored C, N, P cellular composition points to a strongly skewed cell

720 stoichiometry, with low N contents and very low, possibly minimal, P content (**Figure 7**). The
721 synthesis of hydrolytic enzymes was therefore likely impaired by the lack of nutrients and
722 cellular reserves. We suspect that the prolonged stress conditions had brought cultures in such
723 a P-depleted state that cells could no longer devote sufficient energy (ATP) and possibly also
724 nitrogen to sustaining an active synthesis of hydrolytic enzymes. But as we added DOP, APA
725 was soon restored. We postulate that the APA level that we measured at the end of the P_i-
726 depleted phase, although much lower than that we measured three days after the addition of
727 DOP, was not null. Some enzymes may also have remained active for a few days. This activity
728 must have been sufficient for cells to start acquiring P again, which re-launched both the P and
729 N metabolism, as demonstrated by the wider amplitude of the cellular N and P contents (**Figure**
730 **7**), allowing cells to devote again nutrients to the synthesis of hydrolytic enzymes.

731 If not due to alkaline phosphatases, the hydrolyzing activity of DOPs in *Crocospaera* might
732 be attributed to enzymes such as nucleotidases or glycerol phosphatases, should these be able
733 to cleave MUF-P. The genes encoding these enzymes were transcribed in our experiments, but
734 their sequences lack periplasmic targeting sequences (**Supporting information Table S3**).
735 Given that the MUF-P reagent does not penetrate cells and only reacts with periplasmic or
736 extracellular enzymes (60), we conclude that the identified nucleotidases or glycerol
737 phosphatases are unlikely to be the source of the measured APA activity in healthy cells, whose
738 membrane is intact. However, we cannot completely rule out the fact that, in such stressful
739 conditions, in particular after days of P_i starvation, part of the population may have presented
740 altered membranes or entered apoptosis. If the cellular content of some cells was released into
741 the environment, then the APA assay might in part reflect the activity of nucleotidases or
742 glycerol phosphatases.

743 Recently, a novel alkaline phosphatase enzyme (called Psip), which shares low sequence
744 similarity with the PhoA, D, V, and X enzymes, was identified in some *Prochlorococcus* and
745 *Synechococcus* strains (47). This enzyme had initially been designated Psip1 (for Phosphate-
746 induced protein 1 (30). We discovered an ortholog of *psip1* exclusively in the genome of *C.*
747 *chwakensis*. Therefore, the related enzyme cannot either be responsible for the DOP hydrolytic
748 activity observed in our experiment on *C. watsonii* WH8501. Note that the name Psip is also
749 used in the literature for a transcriptional regulator involved in P_i stress signaling in the
750 annotation of *C. watsonii* genome (**Figure 1**). The multiple use of a same name for an enzyme
751 and a regulator, as well as annotation errors (as pointed out above for *phoA*), are the source of
752 biases and confusion in the current databases. This underscores the need for improved
753 annotation of P_i-related genes in cyanobacterial genomes.

754 In *C. watsonii* cultures, the transcription of genes involved in P_i uptake (*som*, *sphX*, *pstS*, *ugpC*),
755 signaling (*ptrA*), and DOP utilization (5'nucleotidase, *ugpQ*, *phoX*) during a period of P_i
756 limitation, and in response to DOP addition (**Figure 4, Supporting information Figure S1**),
757 demonstrates that the induction of these genes mediates the adaptive response to this stress.
758 This response also resulted in changes in physiological parameters, such as cell size and
759 elemental C, N, P contents (**Figures 6, 7**). The survival of the cultures throughout the long, P_i
760 starvation period as indicated by the relatively stable cell abundance, higher average C:N ratio
761 and collapsed N:P ratio, reflects a certain metabolic resilience facing P_i depletion over several
762 generation times (**Figure 6, Table 1**). The pseudo-cyclic increases and decreases in cell volume,
763 C, N, P contents and skewed C:N and N:P ratios observed at the end of the P_i-depleted phase
764 altogether indicate that under phosphorus starvation, cells managed to maintain a basal activity
765 but showed a relative inability to divide. If some cell division occurred, it could at most
766 compensate for cell decay (**Figure 7, Table 1**). All the measured physiological parameters
767 indicate that cells maintained their viability during the limitation period. The restored diel

768 cyclicity and cells C, N, P contents at the end of the experiment reinforce this conclusion,
769 demonstrating a recovery of growth supported by the DOP addition (**Figures 6, 7**). These
770 findings reveal the metabolic resilience of *C. watsonii* and underscore the profound impact of
771 P_i stress on both energetic processes and nitrogen metabolism. Additionally, they illustrate the
772 crucial role of P_i stress-response genes in this adaptive strategy.

773

774 **References**

775

- 776 1. Zehr JP, Capone DG. 2020. Changing perspectives in marine nitrogen fixation. *Science* 368.
- 777 2. Karl DL, R. Tupas, L. Dore, J. Christian, J. Hebel, D. 1997. The role of nitrogen fixation in
778 biogeochemical cycling in the subtropical North Pacific Ocean. *NATURE* 388:533–538.
- 779 3. Sohm JA, Webb EA, Capone DG. 2011. Emerging patterns of marine nitrogen fixation. *Nat Rev*
780 *Microbiol* 9:499-508.
- 781 4. Abed RM, Dobretsov S, Sudesh K. 2009. Applications of cyanobacteria in biotechnology. *J*
782 *Appl Microbiol* 106:1-12.
- 783 5. Zehr JP, Waterbury JB, Turner PJ, Montoya JP, Omoregie E, Steward GF, Hansen A, Karl DM.
784 2001. Unicellular cyanobacteria fix N₂ in the subtropical North Pacific Ocean. *Nature*
785 412:635-8.
- 786 6. Bench SR, Heller P, Frank I, Arciniega M, Shilova IN, Zehr JP. 2013. Whole genome
787 comparison of six *Crocospaera watsonii* strains with differing phenotypes. *J Phycol* 49:786-
788 801.
- 789 7. Mares J, Johansen JR, Hauer T, Zima J, Jr., Ventura S, Cuzman O, Tiribilli B, Kastovsky J. 2019.
790 Taxonomic resolution of the genus *Cyanothece* (Chroococcales, Cyanobacteria), with a
791 treatment on *Gloeothece* and three new genera, *Crocospaera*, *Rippkaea*, and *Zehria*. *J*
792 *Phycol* 55:578-610.
- 793 8. Moutin T, Van Den B, B., Beker, B., Dupouy, C., Rimmelin, P., Le Bouteiller, A.,. 2005.
794 Phosphate availability controls *Trichodesmium* spp. biomass in the SW Pacific Ocean. *Mar*
795 *Ecol Prog Ser* 297:15–21.
- 796 9. Turk-Kubo KA, Achilles KM, Serros TR, Ochiai M, Montoya JP, Zehr JP. 2012. Nitrogenase
797 (*nifH*) gene expression in diazotrophic cyanobacteria in the Tropical North Atlantic in
798 response to nutrient amendments. *Front Microbiol* 3:386.
- 799 10. Rao NN, Torriani A. 1990. Molecular aspects of phosphate transport in *Escherichia coli*. *Mol*
800 *Microbiol* 4:1083-90.
- 801 11. Yamane K, Maruo B. 1978. Alkaline phosphatase possessing alkaline phosphodiesterase
802 activity and other phosphodiesterases in *Bacillus subtilis*. *J Bacteriol* 134:108-14.
- 803 12. Wu JR, Shien JH, Shieh HK, Hu CC, Gong SR, Chen LY, Chang PC. 2007. Cloning of the gene and
804 characterization of the enzymatic properties of the monomeric alkaline phosphatase (*PhoX*)
805 from *Pasteurella multocida* strain X-73. *FEMS Microbiol Lett* 267:113-20.
- 806 13. Santos-Beneit F. 2015. The *Pho* regulon: a huge regulatory network in bacteria. *Front*
807 *Microbiol* 6:402.
- 808 14. Rabouille S, Tournier L, Duhamel S, Claquin P, Crispi O, Talec A, Landolfi A, Oschlies A. 2022.
809 Organic Phosphorus Scavenging Supports Efficient Growth of Diazotrophic Cyanobacteria
810 Under Phosphate Depletion. *Front Microbiol* 13:848647.

- 811 15. Dyhrman ST, Haley ST. 2006. Phosphorus scavenging in the unicellular marine diazotroph
812 *Crocospaera watsonii*. *Appl Environ Microbiol* 72:1452-8.
- 813 16. Pereira N, Shilova IN, Zehr JP. 2016. Molecular markers define progressing stages of
814 phosphorus limitation in the nitrogen-fixing cyanobacterium, *Crocospaera*. *J Phycol* 52:274-
815 82.
- 816 17. Pereira N, Shilova IN, Zehr JP. 2019. Use of the high-affinity phosphate transporter gene,
817 *pstS*, as an indicator for phosphorus stress in the marine diazotroph *Crocospaera watsonii*
818 (*Chroococcales*, *Cyanobacteria*). *J Phycol* 55:752-761.
- 819 18. Shi T, Ilikchyan I, Rabouille S, Zehr JP. 2010. Genome-wide analysis of diel gene expression in
820 the unicellular N(2)-fixing cyanobacterium *Crocospaera watsonii* WH 8501. *ISME J* 4:621-32.
- 821 19. Kondo T, Ishiura M. 2000. The circadian clock of cyanobacteria. *Bioessays* 22:10-5.
- 822 20. Chen YB, Zehr, J. P., Mellon, M. 1996. Growth and nitrogen fixation of the diazotrophic
823 filamentous nonheterocystous cyanobacterium *Trichodesmium* sp. *Ims 101* in defined media:
824 evidence for a circadian rhythm. *Journal of Phycology* 32:916-923.
- 825 21. Gundersen K, Heldal, M., Norland, S., Purdie, D. A., & Knap, A. H. 2002. Elemental C, N, and P
826 cell content of individual bacteria collected at the Bermuda Atlantic Time-series Study (BATS)
827 site. *Limnology and Oceanography* 47:1525-1530.
- 828 22. Hoppe HG. 2003. Phosphatase activity in the sea. *Hydrobiologia*:493.
- 829 23. Lorrain A, Savoye, N., Chauvaud, L., Paulet, Y. M., Naulet, N. 2003. Decarbonation and
830 preservation method for the analysis of organic C and N contents and stable isotope ratios of
831 low-carbonated suspended particulate material. *Analytica Chimica Acta* 491:125-133.
- 832 24. Pujol-Pay M, & Raimbault, P. 1994. Improvement of the wet-oxidation procedure for
833 simultaneous determination of particulate organic nitrogen and phosphorus collected on
834 filters. *Marine Ecology-Progress Series* 105:203.
- 835 25. Holmes RM, Aminot, A., K rouel, R., Hooker, B. A., & Peterson, B. J. 1999. A simple and
836 precise method for measuring ammonium in marine and freshwater ecosystems. *Canadian*
837 *Journal of Fisheries and Aquatic Sciences* 56: 1801-1808.
- 838 26. Mistry J, Finn RD, Eddy SR, Bateman A, Punta M. 2013. Challenges in homology search:
839 HMMER3 and convergent evolution of coiled-coil regions. *Nucleic Acids Res* 41:e121.
- 840 27. Altschul SF, Gish W, Miller W, Myers EW, Lipman DJ. 1990. Basic local alignment search tool.
841 *J Mol Biol* 215:403-10.
- 842 28. Steed PM, Wanner BL. 1993. Use of the rep technique for allele replacement to construct
843 mutants with deletions of the *pstSCAB-phoU* operon: evidence of a new role for the PhoU
844 protein in the phosphate regulon. *J Bacteriol* 175:6797-809.
- 845 29. Rice CD, Pollard JE, Lewis ZT, McCleary WR. 2009. Employment of a promoter-swapping
846 technique shows that PhoU modulates the activity of the PstSCAB2 ABC transporter in
847 *Escherichia coli*. *Appl Environ Microbiol* 75:573-82.
- 848 30. Ostrowski M, Mazard S, Tetu SG, Phillippy K, Johnson A, Palenik B, Paulsen IT, Scanlan DJ.
849 2010. *PtrA* is required for coordinate regulation of gene expression during phosphate stress
850 in a marine *Synechococcus*. *ISME J* 4:908-21.
- 851 31. Umeda H, Aiba H, Mizuno T. 1996. *SomA*, a novel gene that encodes a major outer-
852 membrane protein of *Synechococcus* sp. PCC 7942. *Microbiology (Reading)* 142 (Pt 8):2121-
853 8.
- 854 32. Korteland J, Tommassen J, Lugtenberg B. 1982. PhoE protein pore of the outer membrane of
855 *Escherichia coli* K12 is a particularly efficient channel for organic and inorganic phosphate.
856 *Biochim Biophys Acta* 690:282-9.
- 857 33. Aiba H, Mizuno T. 1994. A novel gene whose expression is regulated by the response-
858 regulator, *SphR*, in response to phosphate limitation in *Synechococcus* species PCC7942. *Mol*
859 *Microbiol* 13:25-34.
- 860 34. Kim SK, Makino K, Amemura M, Shinagawa H, Nakata A. 1993. Molecular analysis of the
861 *phoH* gene, belonging to the phosphate regulon in *Escherichia coli*. *J Bacteriol* 175:1316-24.

- 862 35. Villanueva L, Bale N, Hopmans EC, Schouten S, Damste JS. 2014. Diversity and distribution of
863 a key sulpholipid biosynthetic gene in marine microbial assemblages. *Environ Microbiol*
864 16:774-87.
- 865 36. Rosen BP. 2002. Biochemistry of arsenic detoxification. *FEBS Lett* 529:86-92.
- 866 37. Ishiura M, Kutsuna S, Aoki S, Iwasaki H, Andersson CR, Tanabe A, Golden SS, Johnson CH,
867 Kondo T. 1998. Expression of a gene cluster kaiABC as a circadian feedback process in
868 cyanobacteria. *Science* 281:1519-23.
- 869 38. Kondo T, Ishiura M. 1999. The circadian clocks of plants and cyanobacteria. *Trends Plant Sci*
870 4:171-176.
- 871 39. Takai N, Nakajima M, Oyama T, Kito R, Sugita C, Sugita M, Kondo T, Iwasaki H. 2006. A KaiC-
872 associating SasA-RpaA two-component regulatory system as a major circadian timing
873 mediator in cyanobacteria. *Proc Natl Acad Sci U S A* 103:12109-14.
- 874 40. Dron A, Rabouille S, Claquin P, Le Roy B, Talec A, Sciandra A. 2012. Light-dark (12:12) cycle of
875 carbon and nitrogen metabolism in *Crocospaera watsonii* WH8501: relation to the cell
876 cycle. *Environ Microbiol* 14:967-81.
- 877 41. Dron A, Rabouille S, Claquin P, Talec A, Raimbault V, Sciandra A. 2013. Photoperiod length
878 paces the temporal orchestration of cell cycle and carbon-nitrogen metabolism in
879 *Crocospaera watsonii*. *Environ Microbiol* 15:3292-304.
- 880 42. Webb EA, Ehrenreich IM, Brown SL, Valois FW, Waterbury JB. 2009. Phenotypic and
881 genotypic characterization of multiple strains of the diazotrophic cyanobacterium,
882 *Crocospaera watsonii*, isolated from the open ocean. *Environ Microbiol* 11:338-48.
- 883 43. Rabouille S, Cabral, G.S., Pedrotti, M.L. 2017. Towards a carbon budget of the diazotrophic
884 cyanobacterium *Crocospaera*: effect of irradiance. *Mar Ecol Prog Ser* 570:29-40.
- 885 44. Ray JM, Bhaya D, Block MA, Grossman AR. 1991. Isolation, transcription, and inactivation of
886 the gene for an atypical alkaline phosphatase of *Synechococcus* sp. strain PCC 7942. *J*
887 *Bacteriol* 173:4297-309.
- 888 45. Scanlan DJ, Ostrowski M, Mazard S, Dufresne A, Garczarek L, Hess WR, Post AF, Hagemann
889 M, Paulsen I, Partensky F. 2009. Ecological genomics of marine picocyanobacteria. *Microbiol*
890 *Mol Biol Rev* 73:249-99.
- 891 46. Tetu SG, Brahmasha B, Johnson DA, Tai V, Phillippy K, Palenik B, Paulsen IT. 2009. Microarray
892 analysis of phosphate regulation in the marine cyanobacterium *Synechococcus* sp. WH8102.
893 *ISME J* 3:835-49.
- 894 47. Torcello-Requena A, Murphy ARJ, Lidbury I, Pitt FD, Stark R, Millard AD, Puxty RJ, Chen Y,
895 Scanlan DJ. 2024. A distinct, high-affinity, alkaline phosphatase facilitates occupation of P-
896 depleted environments by marine picocyanobacteria. *Proc Natl Acad Sci U S A*
897 121:e2312892121.
- 898 48. Mohr W, Intermaggio MP, LaRoche J. 2010. Diel rhythm of nitrogen and carbon metabolism
899 in the unicellular, diazotrophic cyanobacterium *Crocospaera watsonii* WH8501. *Environ*
900 *Microbiol* 12:412-21.
- 901 49. Masuda T, Bernat G, Beckova M, Kotabova E, Lawrenz E, Lukes M, Komenda J, Prasil O. 2018.
902 Diel regulation of photosynthetic activity in the oceanic unicellular diazotrophic
903 cyanobacterium *Crocospaera watsonii* WH8501. *Environ Microbiol* 20:546-560.
- 904 50. Redfield AC. 1934. On the proportions of organic derivations in sea water and their relation
905 to the composition of plankton. In: James Johnstone Memorial Volume (ed RJ Daniel)
906 University Press of Liverpool, Merseyside, UK 177–192.
- 907 51. Liu J, Zhou L, Ke Z, Li G, Tan Y. 2020. Phosphorus deficiency induced by aluminum in a marine
908 nitrogen-fixing cyanobacterium *Crocospaera watsonii* WH0003. *Chemosphere* 246:125641.
- 909 52. Knapp AN. 2012. The sensitivity of marine N(2) fixation to dissolved inorganic nitrogen. *Front*
910 *Microbiol* 3:374.
- 911 53. Spungin D, Berman-Frank I, Levitan O. 2014. *Trichodesmium*'s strategies to alleviate
912 phosphorus limitation in the future acidified oceans. *Environ Microbiol* 16:1935-47.

- 913 54. Rouco M, Frischkorn KR, Haley ST, Alexander H, Dyhrman ST. 2018. Transcriptional patterns
914 identify resource controls on the diazotroph *Trichodesmium* in the Atlantic and Pacific
915 oceans. *ISME J* 12:1486-1495.
- 916 55. Frischkorn KR, Haley ST, Dyhrman ST. 2019. Transcriptional and Proteomic Choreography
917 Under Phosphorus Deficiency and Re-supply in the N(2) Fixing Cyanobacterium
918 *Trichodesmium erythraeum*. *Front Microbiol* 10:330.
- 919 56. Zhang F, Wen Z, Wang S, Tang W, Luo YW, Kranz SA, Hong H, Shi D. 2022. Phosphate
920 limitation intensifies negative effects of ocean acidification on globally important nitrogen
921 fixing cyanobacterium. *Nat Commun* 13:6730.
- 922 57. Cerdan-Garcia E, Baylay A, Polyviou D, Woodward EMS, Wrightson L, Mahaffey C, Lohan MC,
923 Moore CM, Bibby TS, Robidart JC. 2022. Transcriptional responses of *Trichodesmium* to
924 natural inverse gradients of Fe and P availability. *ISME J* 16:1055-1064.
- 925 58. Acker M, Hogle SL, Berube PM, Hackl T, Coe A, Stepanauskas R, Chisholm SW, Repeta DJ.
926 2022. Phosphonate production by marine microbes: Exploring new sources and potential
927 function. *Proc Natl Acad Sci U S A* 119:e2113386119.
- 928 59. Lockwood S, Greening C, Baltar F, Morales SE. 2022. Global and seasonal variation of marine
929 phosphonate metabolism. *ISME J* 16:2198-2212.
- 930 60. Luo H, Benner R, Long RA, Hu J. 2009. Subcellular localization of marine bacterial alkaline
931 phosphatases. *Proc Natl Acad Sci U S A* 106:21219-23.

932

933

934

935

936 Figures legends

937 **Figure 1.** Heatmap representation of the number of P_i-related gene orthologs within the 8 *Crocospaera*
938 genomes. The color scale and associated number from 0 to >= 3 represent the number of homologs
939 found in each genome. Grey indicates that no ortholog sequence was found in the genome.
940

941 **Figure 2.** Schematic representation of the distribution of P_i transporters in *Crocospaera*. 1 and 2
942 indicate the number of orthologs in each genome. (-) stands for the absence of ortholog. In each system,
943 the P_i binding periplasmic protein is in green, the membrane subunit(s) in purple, the cytoplasmic
944 ATPase subunits in brown. The figure was drawn using BioRender
945

946 **Figure 3.** Percentage of P_i-related gene orthologs in group of species. The color code based on cell size
947 is shown. Small-cell strains (blue; *C. watsonii* WH8501, WH8502 and WH0401), large-cell strains
948 (orange; *C. watsonii* WH0402, WH0003 and WH0005) and the newly classified strains in the genus
949 (black; *C. subtropica* and *C. chwakensis*).
950

951 **Figure 4.** Relative normalized gene expression of *C. watsonii* WH8501 during the P_i-depleted phase
952 (closed circles, days 1-4) and the DOP-recovery phase (closed triangles, days 8-9). RT-qPCR of the
953 genes encoding for a regulator *ptrA* in purple (A), for a porin *som* in red, and transporters, *sphX* in black,
954 *pstS* in blue, and *ugpC* in grey (B). Expression of the genes encoding for a glycerophosphoesterase *ugpQ*
955 and a 5'-nucleotidase are represented in brown and green, respectively (C). The Y-axis scale is
956 logarithmic. Time on the X axis is expressed in days, starting from the beginning of the high-frequency
957 monitoring phase, i.e. five days after the transfer to a P_i-depleted medium. All points are normalized by
958 the 16S expression at the same point and relative to the first sampling point (Day 1, L0). The horizontal
959 line (y=1) materializes the value of the first sampling point. The expression variability of biological and
960 analytical duplicates is represented by error bars. White and grey shades represent light and dark periods,
961 respectively and red arrows mark the time of DOP addition.
962

963 **Figure 5.** Gene cluster organization and genomic position of *Crocospaera watsonii* WH8501 potential
964 *kaiABC* and percent identity to *Synechococcus elongatus* PCC 7942 (A); relative normalized expression
965 of *C. watsonii* potential circadian clock components *kaiA* (B), *kaiB* (C), *kaiC* (D) and regulator, *rpaA*
966 (E) during the P_i-depleted phase (closed circles) and the DOP-recovery phase (closed triangles). The Y-
967 axes are logarithmic. Time on the X axis is expressed in days, starting from the beginning of the high
968 frequency monitoring phase, i.e. five days after the transfer to a P_i-depleted medium. All points are
969 normalized by the 16S gene expression at the same point and relative to the first sampling point (Day 1,
970 L0). The horizontal line (y=1) materializes the value of the first sampling point. Expression variability
971 of biological duplicates and analytical duplicates are represented by error bars. White and grey shades
972 represent light and dark periods, respectively, and red arrows mark the time of DOP addition.
973

974 **Figure 6.** Diel fluctuations in *C. watsonii* cell abundance (top panel, $\times 10^6$ cells mL⁻¹) and cell biovolume
975 (bottom panel, μm^3 cell⁻¹) represented for each culture replicate (blue, yellow, and C: green). Time on
976 the X axis is expressed in days, starting from the beginning of the high-frequency monitoring phase, i.e.
977 five days after the transfer to a P_i-depleted medium. The dotted lines represent sampling in the first
978 culture triplicate and continuous lines represent samples taken in the second triplicate (see methods).
979 The red arrow marks the time of DOP addition in the second triplicate; sampling of the DOP-recovery
980 phase was performed during Days 8 and 9. White and grey shades represent light and dark periods,
981 respectively.
982

983 **Figure 7.** Diel fluctuations of *C. watsonii* C, N and P cell contents in each replicate (blue, yellow and
984 green) during the P_i-depleted (Day 1 to Day 4) and DOP-recovery (Day 8 and Day 9) phases. Particulate
985 organic carbon (POC, fmol C cell⁻¹, A) and particulate organic nitrogen (PON_c, fmol N cell⁻¹, C) were
986 used to estimate the C:N ratio (mol:mol, E). Particulate organic nitrogen (PON_{oxi}, fmol N cell⁻¹, B) and
987 particulate organic phosphorus (POP, fmol P cell⁻¹, D) were used to estimate the N:P ratio (F). PON_c
988 and PON_{oxi} refer to the complete combustion method and the wet oxidation method, respectively (see
989 methods). Each content was normalized by the cell abundance estimated at the same time point. Time
990 on the X axis is expressed in days, starting from the beginning of the high-frequency monitoring phase,
991 five days after the transfer to a P_i-depleted medium. The dotted lines represent sampling in the first
992 culture triplicate and continuous lines represent samples taken in the second triplicate (see methods).
993 The red arrow indicates the time of DOP addition. The dashed horizontal line represents the Redfield
994 ratio. White and grey shades represent light and dark periods, respectively.
995
996

997 **Table 1.** Dissolved nutrient concentrations (μmol N or P L⁻¹) and per-cell alkaline phosphatase
998 activities (APA, fmol cell⁻¹ h⁻¹) in replicates A, B, and C. In the P_i-depleted phase, values varied
999 little between dark-light (D/L) and light-dark (L/D) transitions, and so were averaged ± standard
1000 deviation in the culture over the entire monitored period. In the DOP-recovery phase,
1001 macronutrient concentrations are reported for the dark-light (D/L) and light-dark (L/D)
1002 transitions of days 8 and 9, and the APA at L3 and D3.

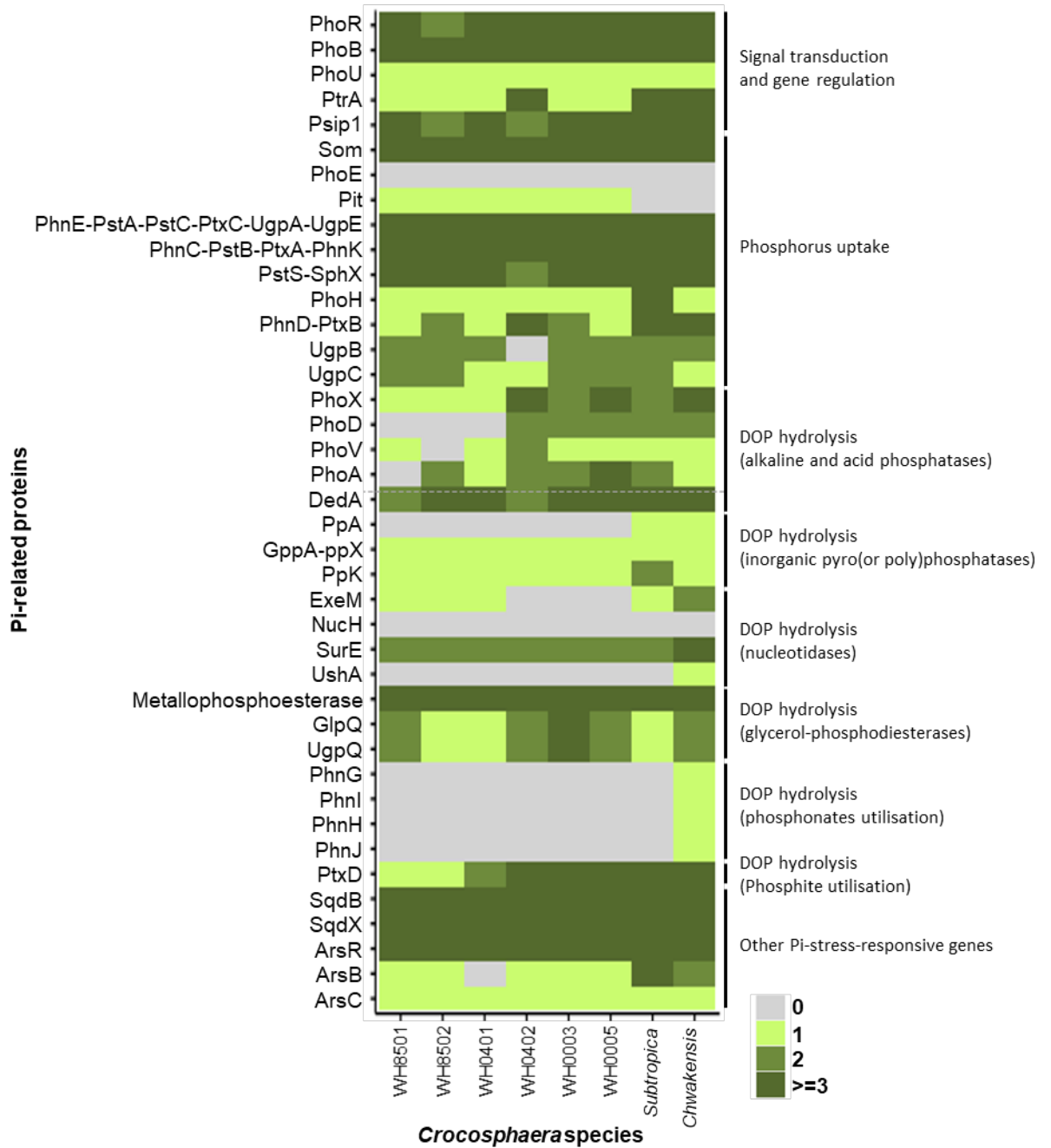
1003

1004

1005

1006 **Main Figures and Tables**

1007



1008

1009

1010 **Figure 1**

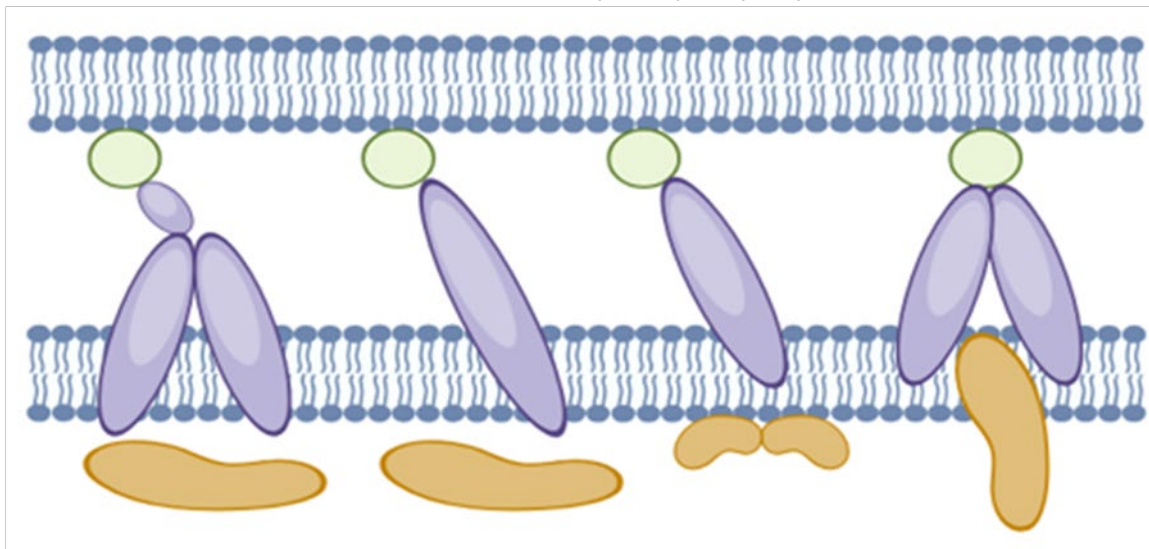
1011

1012

1013

1014

	Phosphate				Phosphite			Phosphonate				Glycerolphosphate			
	PstS/SphX	PstA	PstC	PstB	PtxB	PtxC	PtxA	PhnD	PhnE	PhnC	PhnK	UgpB	UgpA	UgpE	UgpC
WH8501	1/1	1	1	2	-	-	1	-	-	1	1	1	1	1	1
WH8502	1/1	1	1	1	-	-	1	-	-	1	1	1	1	1	1
WH0401	1/1	1	1	1	-	-	1	-	-	1	1	1	1	1	1
WH0402	1/1	1	1	1	-	-	1	-	-	1	1	1	1	1	1
WH0003	1/1	1	1	1	-	-	1	-	-	1	1	1	1	1	1
WH0005	1/1	1	1	1	-	-	1	-	-	1	1	1	1	1	1
<i>subtropica</i>	1/1	1	1	1	1	1	1	1	1	1	1	1	1	1	1
<i>chwakensis</i>	1/1	1	1	1	1	1	1	1	1	1	1	1	1	1	1

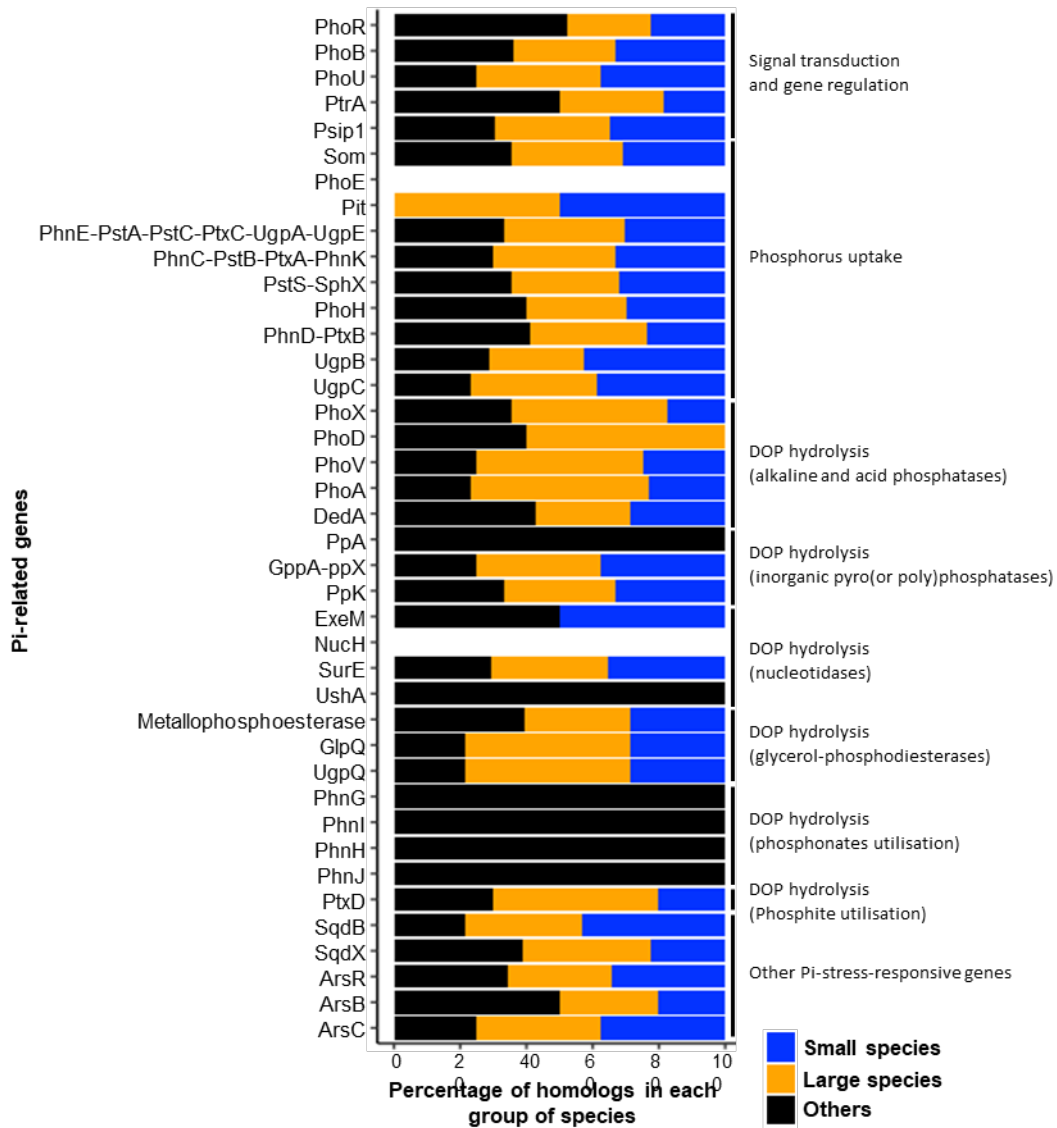


1015

1016

1017 **Figure 2**

1018



1019

1020 **Figure 3**

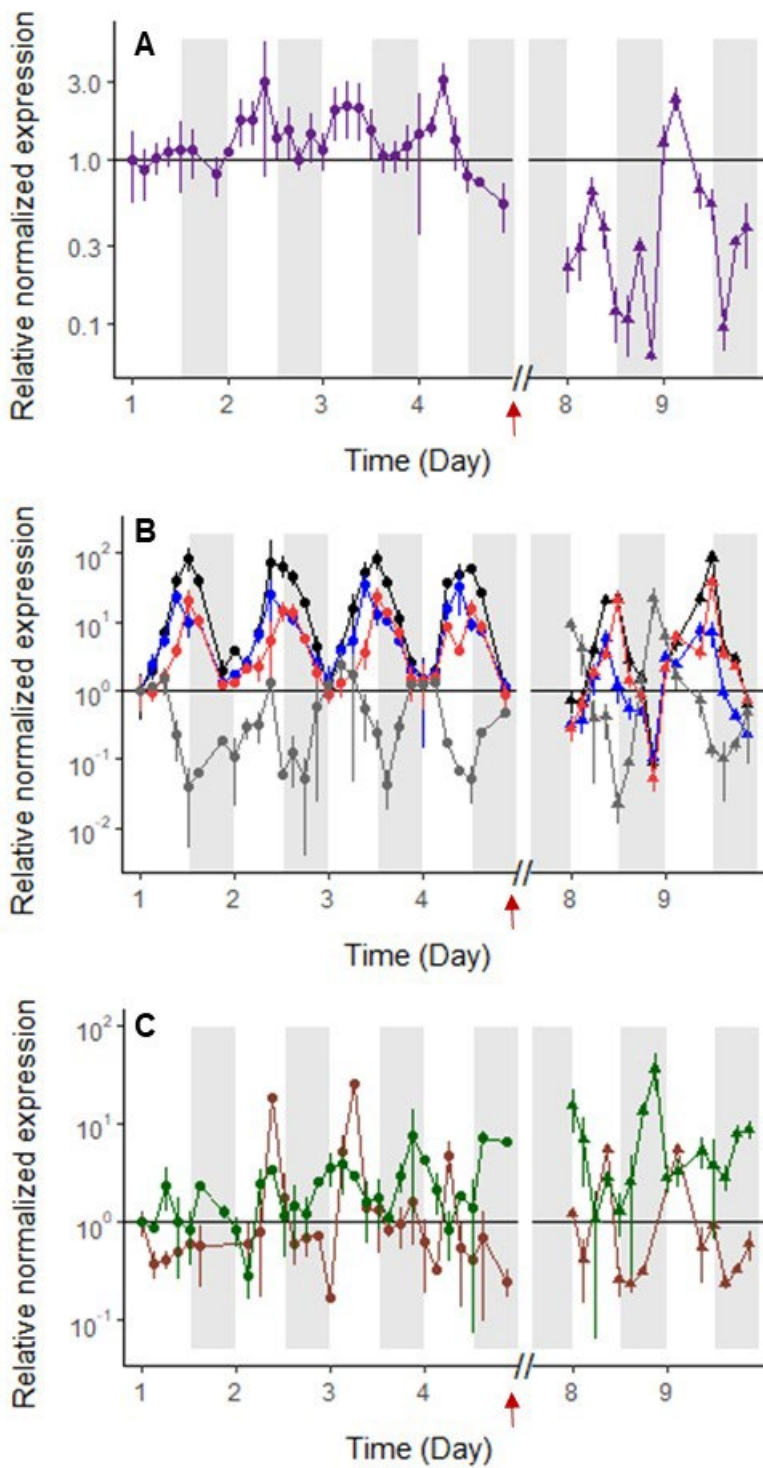
1021

1022

1023

1024

1025



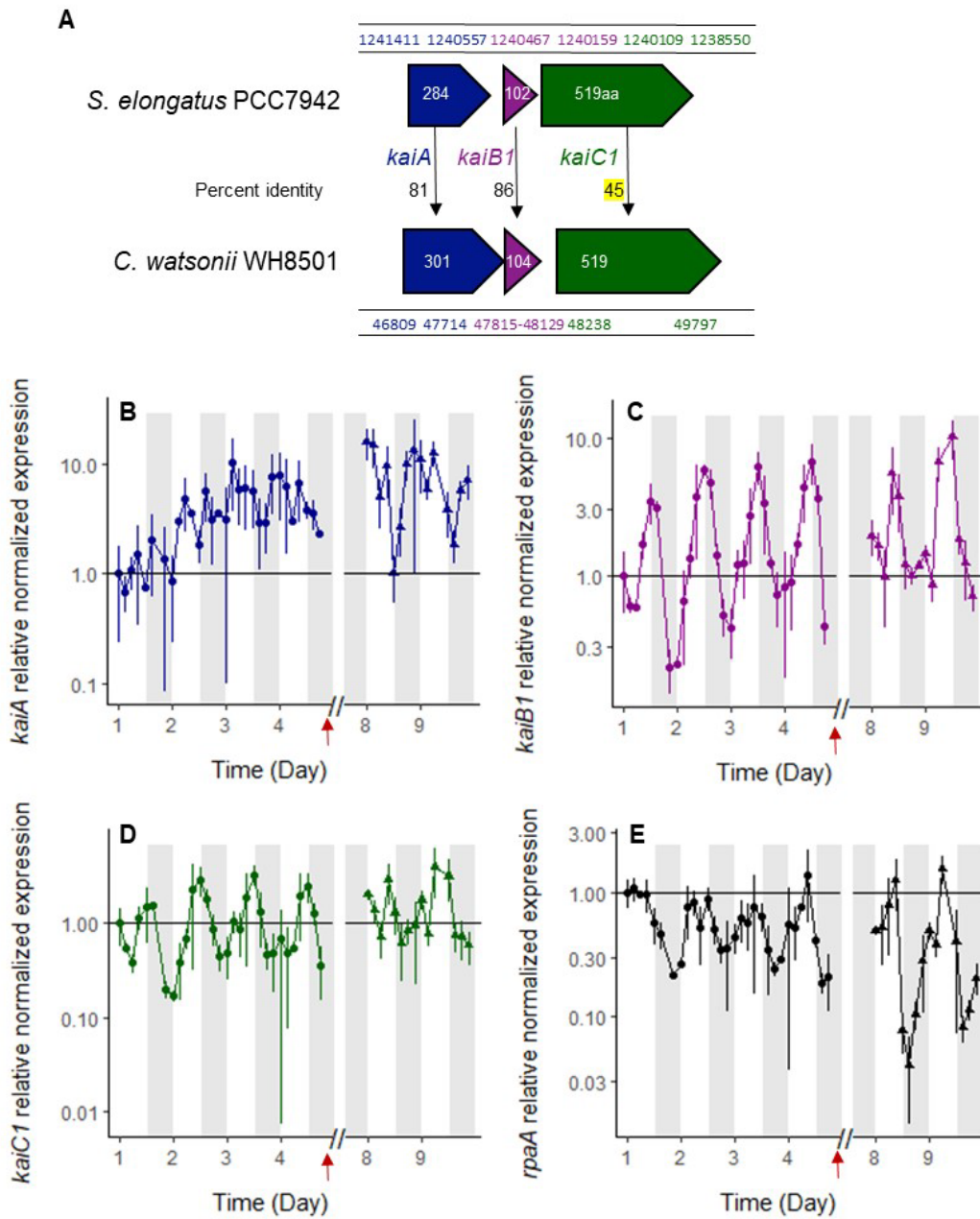
1026

1027

1028 **Figure 4**

1029

1030



1031

1032

1033 **Figure 5**

1034

1035

1036

1037

1038

1039

1040

1041

1042

1043

1044

1045

1046

1047

1048

1049

1050

1051

1052

1053

1054

1055

1056

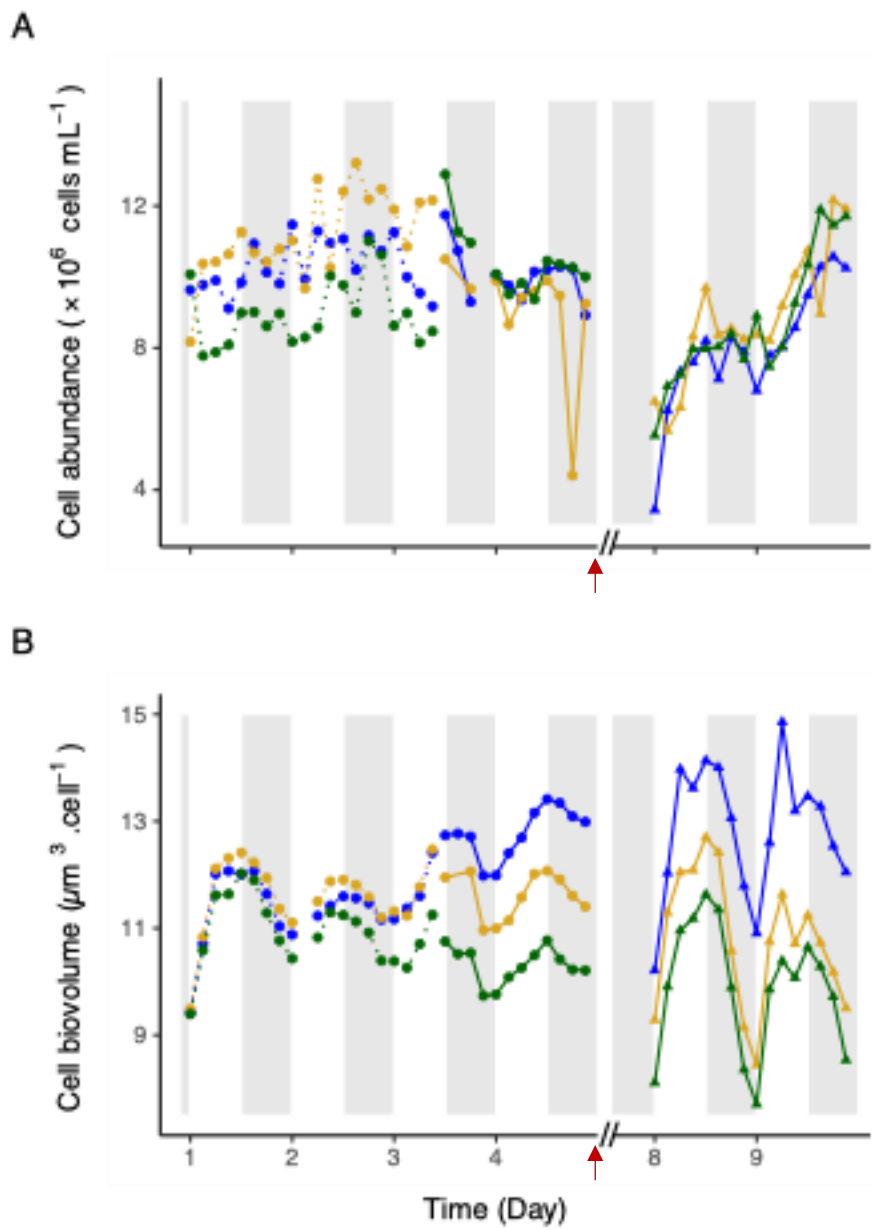
1057

1058

1059 **Figure 6**

1060

1061



1062

1063

1064

1065

1066

1067

1068

1069

1070

1071

1072

1073

1074

1075

1076

1077

1078

1079

1080

1081

1082

1083

1084

1085 **Figure 7**

1086

1087

Figure 7 consists of six panels (A-F) showing nutrient concentrations and ratios over time. The x-axis for all panels is 'Time (Day)', with a break between day 4 and day 8 indicated by a red arrow and a double slash (//). Shaded vertical bars represent experimental periods.

- Panel A:** POC (fmol C cell⁻¹) vs Time (Day). Y-axis ranges from 0 to 800. Shows a sharp increase at day 8.
- Panel B:** PON_c (fmol N cell⁻¹) vs Time (Day). Y-axis ranges from 0 to 100. Shows a sharp increase at day 8.
- Panel C:** PON_{ox} (fmol N cell⁻¹) vs Time (Day). Y-axis ranges from 0 to 60. Shows a sharp increase at day 8.
- Panel D:** POP (fmol P cell⁻¹) vs Time (Day). Y-axis ranges from 0 to 6. Shows a sharp increase at day 8.
- Panel E:** C:N ratio vs Time (Day). Y-axis ranges from 6 to 12. A dashed horizontal line is at approximately 6.8. Shows a sharp increase at day 8.
- Panel F:** N:P ratio vs Time (Day). Y-axis ranges from 10 to 30. A dashed horizontal line is at approximately 15. Shows a sharp decrease at day 8.

44

1088 **Table 1.**

1089

	Replicate	P _i -depleted (n=8)	DOP recovery			
			Day8	Day8	Day9	Day9
		D/L and L/D	D/L	L/D	D/L	L/D
Total dissolved phosphorus (TDP)	A	0.21±0.03	3.33	1.71	1.53	0.98
	B	0.20±0.01	5.01	3.84	3.00	1.33
	C	0.21±0.02	3.63	2.10	1.86	0.60
Dissolved organic phosphorus (DOP)	A	0.20±0.03	1.17	0.90	1.16	0.97
	B	0.17±0.02	0.20	0.48	0.34	0.24
	C	0.17±0.02	0.32	0.39	0.15	0.26
Phosphate (PO₄³⁻)	A	0.01±0.00	2.16	0.81	0.37	0.01
	B	0.03±0.01	4.81	3.36	2.66	1.09
	C	0.05±0.02	3.31	1.71	1.71	0.34
Total dissolved nitrogen (TDN)	A	9.62±1.30	18.47	18.39	18.75	19.59
	B	9.36±0.73	21.69	24.42	19.29	18.60
	C	9.35±0.67	19.21	18.64	19.80	19.27
Dissolved organic nitrogen (DON)	A	9.36±1.30	18.17	18.16	18.47	19.37
	B	9.12±0.73	20.60	23.84	18.78	18.02
	C	9.09±0.68	17.55	18.05	19.27	18.94
Nitrate (NO₃⁻)	A	0.26±0.05	0.30	0.23	0.28	0.22
	B	0.24±0.04	1.09	0.58	0.51	0.58
	C	0.26±0.06	1.66	0.59	0.53	0.33
		L3 and D3	L3	D3	L3	D3
APA	A	1.21±0.73	2.56	4.59	3.43	3.28
	B	1.78±0.76	5.47	6.06	5.02	5.83
	C	1.74±0.84	5.43	7.17	5.64	4.38

1090

Appendix

1091 Appendix Supplementary Tables

1092 **Appendix Table S1.** Primer sequences and amplification conditions for the genes used in RT-qPCR

Gene	Primer	Sequence (5'-3')
16S	F	AAAGCTTACCAAGGCGACGA
	R	GAAAATTCCCCACTGCTGCC
5' ND	F	CCCTTGTAGAAACCCACCT
	R	TGTCACCAATCTCCGGCTA
<i>dedA</i>	F	GCCCCTCCCAAGTTACACAA
	R	TTTGGGCGTTTGTACCTT
Metallophosphoesterase	F	ACAAATAGAAGCGATGTGGGC
	R	AGAACCAGAAGCGTCGTGAT
<i>pstS</i>	F	CCGTAGTTCACCGTTCCGAT
	R	AAGCGGTTACCCCTTCGTTT
<i>ptrA</i>	F	TTTGTTAGGTTGGGCGCAAC
	R	ATTCGACGGGCTAACTGACT
<i>som</i>	F	CGTGTGGCTAGTGATCCCTT
	R	CTCCATTAGCCGGGTTAGCA
<i>sphX</i>	F	CGATAATGGGAATGGTGGGGT
	R	AGGATTTTCTTGGGCCCGTT
<i>surE</i>	F	CTTCATCAGCCATTCGTGC
	R	GGTGGGTTTCTACAAGGT
<i>ugpC</i>	F	CTGGGTGTGGCAAAGTACC
	R	ACAGCAGGTTGTCTCAGAT
<i>ugpQ</i>	F	GCCTCTTATAATTGCTCACCGTG
	R	TCAGCTACATTTGTCGTTTCTGA
<i>phoX</i>	F	ACAAAACAAAGGGCTGCAA
	R	AACACACACCAGCAAAGTGG
<i>rpaA</i>	F	ATGTTGCCCAAAGTAGAC
	R	GTTTGACCGTGACGCT
<i>kaiA</i>	F	GGGCGTAGTTGTTGTCTTGC
	R	CGTCCATCAGTCCATGTGC
<i>kaiB</i>	F	CAAACCTCTACGTCGCTGGTAAT

<i>kaiC</i>	R	CCTCATAGAGAAGATCCAAACCA
	F	GATGCAGCTCTGTGGTGAG
	R	GAAGAACTGCGCGCATTA

1093

1094

1095

1096 **Appendix Table S2 (Excell file):**

1097 **Sheet 1. List of *Crocospaera* genomes used in this study.** The cell size features were obtained from
1098 the literature.

1099 **Sheet 2. Protein seeds (or reference proteins) used in this study.** Accession numbers (from Uniprot
1100 www.uniprot.org and Refseq www.ncbi.nlm.nih.gov databases) are indicated as well as the targeted
1101 molecules and the functional domain patterns (see **Experimental procedures**). The targeted molecule
1102 associated to each seed was obtained from the literature. Within the domain patterns, domains are
1103 shown in the order of appearance in the protein and separated with a star (*). Domain abbreviations
1104 and their functional descriptions of the domains are shown in **Sheet 3**. Other data were retrieved from
1105 the Uniprot or NCBI databases. Similar or identical seeds (from distinct organisms) are grouped into
1106 one seed (*e.g.* GppA-PpX).

1107 **Sheet 3. List of functional seed domains**

1108 **Sheet 4. List of protein orthologs.**

1109 **Sheet 5. Distribution of protein orthologs in *Crocospaera* species**

1110 **Sheet 6. Distribution of protein homologs in group of *Crocospaera* species**

1111

1112 **Appendix Table S3: Prediction of cellular location of DOP-hydrolyzing enzymes in *C.***
1113 ***watsonii* WH8501**

1114 The presence of signal peptides Sec or Tat was analyzed using Signal IP-6.01 software
1115 (<https://services.healthtech.dtu.dk/services/SignalP-6.0/>)

Protein	Signal peptide	Type/position (amino acids)	Predicted cellular location
Alcaline phosphatase PhoX	Yes	TAT/ 1-24	Extra-cytosolic
Phosphatase like DedA	No		Cytosolic
5'Nucleotidase SurE	No		Cytosolic
Metallophosphoesterase	No		Cytosolic
Glycerolphosphoesterase UgpQ	No		Cytosolic

1116

1117

1118

1119

1120

1121

1122 Appendix Supplementary Figures

1123

1124

1125

1126

1127

1128

1129

1130

1131

1132

1133

1134

1135

1136

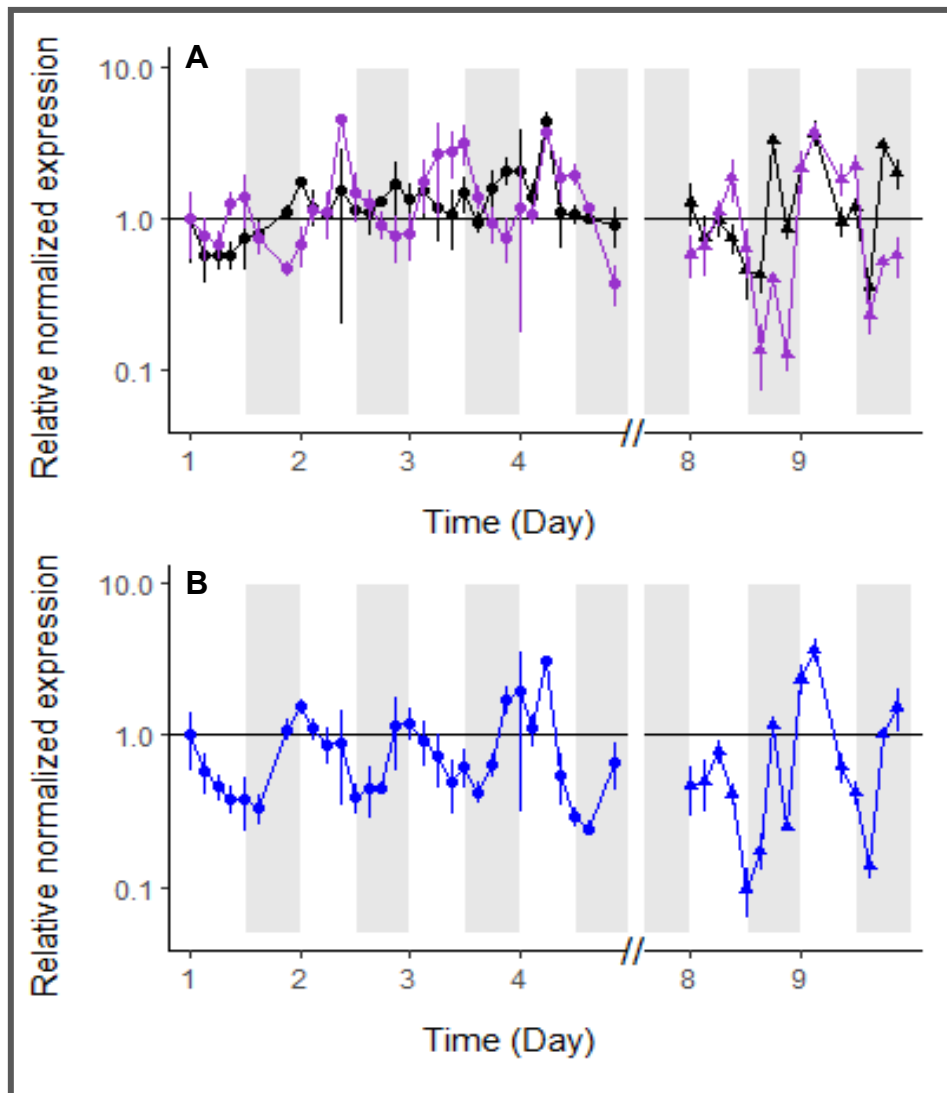
1137

1138

1139

1140

1141



1142

1143

1144

1145

1146

1147

1148

1149

1150

1151

1152

Appendix Figure S1: Relative normalized gene expression of *C. watsonii* during the P_i -depleted phase (closed circles, left panels) and the DOP-recovery phase (closed triangles, right panels). RT-qPCR of the genes encoding a potential 5'-nucleotidase, *surE* (in black, **A**), a metallophosphoesterase (in purple), and the alkaline phosphatase-like, *dedA* (in blue, **B**). The Y-axis is logarithmic. All points are normalized by the 16S expression at the same point and relative to the first sampling point (Day 1, L0). Expression variability of biological duplicates and analytical duplicates are represented by error bars. White and grey shades represent the light and dark periods, respectively; red arrows indicate the day of DOP addition.

1153

1154

1155

1156

1157

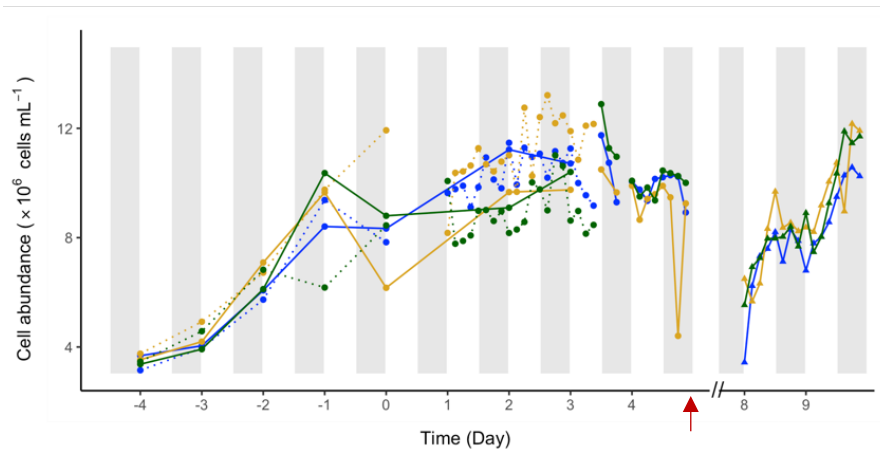
1158

1159

1160

1161

1162



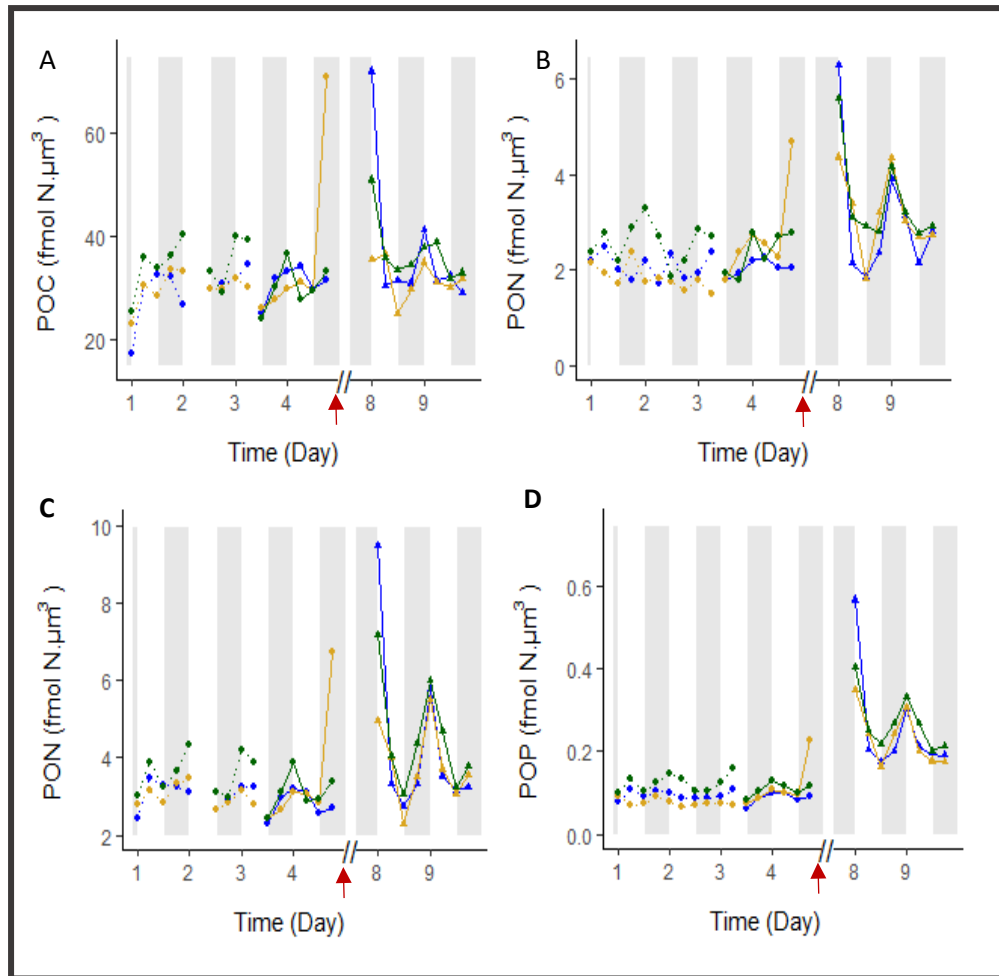
1163

1164

1165

1166 **Appendix Figure S2:** Diel fluctuations in *C. watsonii* total population cell abundance (cell.mL⁻¹)
1167 measured in each triplicate (blue, yellow and green) over the entire P_i-depleted period. Cultures
1168 were transferred to the P_i-depleted medium on Day -4 and the high-frequency monitoring started on
1169 Day 1. The dotted lines represented sampling in the first triplicate and solid lines samples taken in
1170 the second triplicate. The red arrow marks the day of DOP addition and samples of the DOP-recovery
1171 phase were realized Days 8 and 9.

1172
1173
1174
1175
1176
1177
1178
1179
1180
1181
1182
1183
1184
1185
1186
1187
1188
1189



1190 **Appendix Figure S3:** Diel fluctuations of *C. watsonii* C, N and P cell contents in each replicate (blue,
1191 yellow and green) during the P_i-depleted (Day 1 to Day 4) and DOP-recovery (Day 8 and Day 9) phases.
1192 Particulate organic carbon (POC, fmol C μm^{-3} , A) and particulate organic nitrogen (PON_c, fmol N μm^{-3} ,
1193 C) were used to estimate the C:N ratio (mol:mol, E). Particulate organic nitrogen (PON_{oxi}, fmol N μm^{-3} ,
1194 B) and particulate organic phosphorus (POP, fmol P μm^{-3} , D) were used to estimate the N:P ratio (F).
1195 PON_c and PON_{oxi} refer to the complete combustion method and the wet oxidation method, respectively
1196 (see methods). Each content was normalized by the biovolume (μm^{-3}) estimated at the same time point.
1197 Time on the X axis is expressed in days, starting from the beginning of the high-frequency monitoring
1198 phase, five days after the transfer to a P_i-depleted medium. The dotted lines represent sampling in the
1199 first culture triplicate and continuous lines represent samples taken in the second triplicate (see
1200 methods). The red arrow indicates the time of DOP addition. The dashed horizontal line represents the
1201 Redfield ratio. White and grey shades represent light and dark periods, respectively.

1202
1203
1204
1205
1206
1207